

## **Criteria 3**

### **Research, Innovations and Extension**

#### **Key Indicator 3.3**

##### **Research Publication and Awards**

**3.3.1 Number of research papers published per teacher in the Journals notified on UGC website during the last five years**



**Rajarshi Shahu**  
**College of Pharmacy**

Journey Towards Academic Excellence

**3.3.1 Number of research papers published per teacher in the Journals notified on UGC website during the last five years**

**2018-2019**


Sr. No.	Title of paper	Name of the author/s	Department of the teacher	Name of journal	Impact Factor	Page No. with Link
1	Homozygous variants in the HEXB and MBOAT7 genes underlie neurological diseases in consanguineous families	Shazia Khan, Lettie E Rawlins, <b>Gaurav V Harlalka</b> , Muhammad Umair, Asmat Ullah, Shaheen Shahzad, Muhammad Javed, Emma L Baple, Andrew H Crosby, Wasim Ahmad, Asma Gul	Pharmacology	BMC Med Genet (2019) 20:199	1.988	<u><a href="#">01</a></u>
2	Novel nonsense variants in SLURP1 and DSG1 cause palmoplantar keratoderma in Pakistani families	Abida Akbar, Claire Prince, Chloe Payne, James Fasham, Wasim Ahmad, Emma L Baple, Andrew H Crosby, <b>Gaurav V Harlalka</b> , Asma Gul	Pharmacology	BMC Med Genet (2019) 20:145	1.988	<u><a href="#">10</a></u>
3	Glucosamine- HCl based solid dispersion carrier for enhancing biopharmaceutical attributes of acyclovir	<b>D. R. Telange</b> , V.S. Dave, S. B. Bhagat	Pharmaceutics	J. Excipients and Food Chem. 10 (3) 2019, 65-81	0	<u><a href="#">17</a></u>
4	Quality by Design: A Roadmap for Quality Pharmaceutical Products	Mayur Ashok Chordiya, Hemant Hiranman, Gangurde, <b>Vikram Nirmal Sancheti</b>	Pharmaceutics	Journal of Reports in Pharmaceutical Sciences Volume 8   Issue 2, 289	0	<u><a href="#">34</a></u>

RESEARCH ARTICLE

Open Access



# Homozygous variants in the *HEXB* and *MBOAT7* genes underlie neurological diseases in consanguineous families

Shazia Khan<sup>1,2,3</sup>, Lettie E. Rawlins<sup>2,4</sup>, Gaurav V. Harlalka<sup>2,5</sup>, Muhammad Umair<sup>6</sup>, Asmat Ullah<sup>3,7</sup>, Shaheen Shahzad<sup>1</sup>, Muhammad Javed<sup>8</sup>, Emma L. Baple<sup>2,4</sup>, Andrew H. Crosby<sup>2</sup>, Wasim Ahmad<sup>3</sup> and Asma Gul<sup>1\*</sup> 

## Abstract

**Background:** Neurological disorders are a common cause of morbidity and mortality within Pakistani populations. It is one of the most important challenges in healthcare, with significant life-long socio-economic burden.

**Methods:** We investigated the cause of disease in three Pakistani families in individuals with unexplained autosomal recessive neurological conditions, using both genome-wide SNP mapping and whole exome sequencing (WES) of affected individuals.

**Results:** We identified a homozygous splice site variant (NM\_000521:c.445 + 1G > T) in the hexosaminidase B (*HEXB*) gene confirming a diagnosis of Sandhoff disease (SD; type II GM2-gangliosidosis), an autosomal recessive lysosomal storage disorder caused by deficiency of hexosaminidases in a single family. In two further unrelated families, we identified a homozygous frameshift variant (NM\_024298.3:c.758\_778del; p.Glu253\_Ala259del) in membrane-bound O-acyltransferase family member 7 (*MBOAT7*) as the likely cause of disease. *MBOAT7* gene variants have recently been identified as a cause of intellectual disability (ID), seizures and autistic features.

**Conclusions:** We identified two metabolic disorders of lipid biosynthesis within three Pakistani families presenting with undiagnosed neurodevelopmental conditions. These findings enabled an accurate neurological disease diagnosis to be provided for these families, facilitating disease management and genetic counselling within this population. This study consolidates variation within *MBOAT7* as a cause of neurodevelopmental disorder, broadens knowledge of the clinical outcomes associated with *MBOAT7*-related disorder, and confirms the likely presence of a regionally prevalent founder variant (c.758\_778del; p.Glu253\_Ala259del) in Pakistan.

**Keywords:** Neurological disorder, *HEXB*, *MBOAT7*, Exome sequencing, Sandhoff disease, Pakistan

## Background

Neurological disorders cause structural, functional, biochemical or electrical abnormalities in the nervous system, resulting in cognitive impairment, seizures, muscle weakness, paralysis, poor coordination and mood alteration. Neurological disorders are an increasing burden in developing countries due to improving life expectancy, urbanisation of the population and improved health care and diagnosis. A higher prevalence of intellectual disability (ID) and epilepsy have been identified within

Pakistani populations compared with more economically developed countries [1, 2]. In Pakistan, 82.5% of the parents are blood relatives due to religious, economic, social and cultural reasons in different regions [3]. The *HEXB* gene encodes the hexosaminidase beta subunit, which forms a heterodimer with the alpha subunit in hexosaminidase A (HEXA) and a homodimer in hexosaminidase B (HEXB), which are important enzymes within neuronal membrane components responsible for GM2 ganglioside degradation. Sandhoff disease (SD)(MIM 268800) is an autosomal recessive lysosomal lipid storage disorder caused by biallelic variants within the *HEXB* gene, resulting in deficiency of HEXA and HEXB enzymes [4] and intralysosomal accumulation of GM2

\* Correspondence: [gulasma@iiu.edu.pk](mailto:gulasma@iiu.edu.pk)

<sup>1</sup>Department of Biological Sciences, International Islamic University Islamabad, H-10, Islamabad 44000, Pakistan

Full list of author information is available at the end of the article



ganglioside and related glycolipids within neurons. This leads to progressive destruction of the central nervous system (CNS); classical onset of SD occurs with onset of symptoms before 6 months of age of progressive psychomotor retardation, motor weakness, hyperreflexia, early blindness with cherry red spots, macrocephaly, and with death occurring by 3–5 years [5].

Recently homozygous pathogenic variants within *MBOAT7* have been identified in 16 families (15 consanguineous and 1 reported as non-consanguineous, although both parents were from the same village in Lebanon) as a cause of a neurodevelopmental disorder (autosomal recessive mental retardation type 57 (MIM 617188) characterized by seizures, moderate to severe ID with significant psychomotor retardation (several individuals are non-verbal and never walked, usually occurring with seizure onset), truncal hypotonia, appendicular hypertonia, features of autism spectrum disorder (ASD), below average head circumference and characteristic facial features [6–10]. The *MBOAT* protein family consists of five acyltransferases; lysophosphatidylinositol acyltransferase 1 (LPIAT1) encoded by the *MBOAT7* gene is known to transfer arachidonic acid (AA) from arachidonoyl-CoA to lysophosphatidylinositol [11]. Only one other *MBOAT* gene has been linked to human disease of brachydactyly-syndactyly syndrome in a single

patient with a balanced translocation disrupting *MBOAT1* [12].

In the present study, we investigate three consanguineous Pakistani families with features of autosomal recessive neurological disorders in order to identify a precise molecular diagnosis using a combination of genome wide SNP mapping and whole exome sequencing (WES).

**Methods**

**Ethics approval and consent to participate**

This study was approved by the Institutional Ethical Review Board of International Islamic University, Islamabad, Pakistan. Written informed consent to participate was obtained from all individuals in the study or their parents.

Three families were recruited to the study from remote regions of Khyber Pakhtunkhwa (KP) province of Pakistan. Available affected and unaffected members of all families underwent clinical examination at local government hospitals with review of relevant medical records and blood samples were taken with informed consent.

**Genomic analysis**

Venous blood samples were collected in EDTA tubes (BD, Franklin Lakes, NJ, USA) from 15 individuals (shown with asterisks; Fig. 1) and DNA was extracted

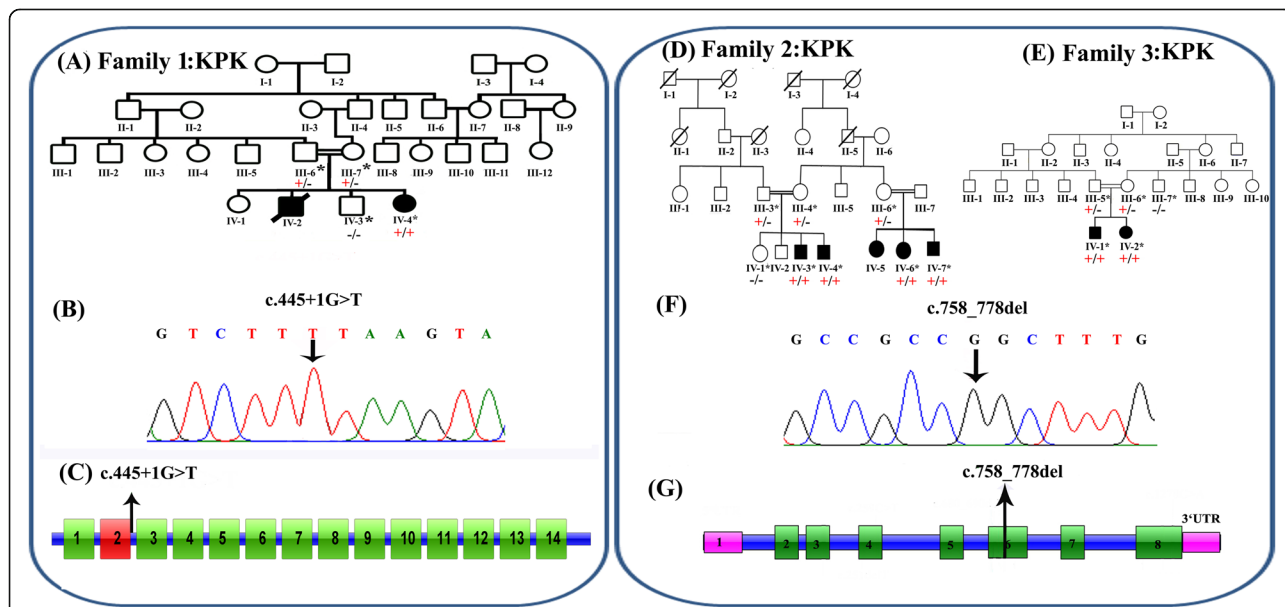


**Fig. 1 a** Pedigree of family 1, with two affected siblings with Sandhoff disease (filled symbols). Genotype is shown in red under individuals (+, mutant; -, WT). \* indicates samples available for analysis. The affected female was shown to be homozygous for the *HEXB* c.445 + 1G > T splice site variant. **b** Electropherogram showing the DNA sequence variant (*HEXB* c.445 + 1G > T) in a homozygous affected individual. **c** Schematic representation of *HEXB* exons and position of the genomic variant identified in this study. **d-e** Pedigrees of families 2 and 3, both from the Khyber Pakhtunkhwa province and with individuals affected with a neurodevelopmental disorder (filled symbols), within the same generation. Genotype is shown in red under individuals (+, mutant; -, WT). \* indicates samples available for analysis. Six affected individuals were shown to be homozygous for the *MBOAT7* c.758\_778del; p.(Glu253\_Ala259del) variant **f** Electropherogram showing the DNA sequence variant (*MBOAT7* c.758\_778del; p.(Glu253\_Ala259del) in a homozygous affected individual **g** Schematic representation of *MBOAT7* exons and positions of the genomic variant identified in this study

using the GenElute™ Blood Genomic DNA Kit (Merck) according to the manufacturer's protocols and quantification using standard methods. WES was undertaken on DNA from a single affected individual of family A (IV-2) using the Agilent 2100 Bioanalyser/Illumina HiSeq2000 platform and exome enrichment was performed using SureSelect Human All ExonV4 (51 Mb) with a mean read depth of 30X. Reads were aligned (BWA-MEM), mate-pairs fixed and duplicates removed (Picard), inDel realignment and base quality recalibration performed (GATK). SNVs and InDels were detected using GATK HaplotypeCaller and custom annotation was performed using standard DNAnexus (DNAnexus Inc., Mountain View, CA; <https://dnanexus.com>). Data was filtered to identify rare non-synonymous exonic or splice variants, with a population frequency of < 0.01 in control databases (including the Genome Aggregation Database; gnomAD, the Exome Aggregation Consortium; ExAC, and the 1000 Genomes Project), and analysed considering the disease phenotype. Single-nucleotide polymorphism (SNP) genotyping was performed (HumanCytoSNP-12 v2.1 beadchip array, Illumina) in 3 affected individuals in family B. In silico prediction of variant pathogenicity was assessed using FATHMM (<http://fathmm.biocompute.org.uk/>), MutationTaster (<http://www.mutationtaster.org/>), Varsome (<https://varsome.com/>), DaNN (<https://omictools.com/dann-tool>), NNSplice (Berkeley, CA, USA), MutPred Splice (v1.3.2), MaxEnt, SKIPPY and Human Splice Finder (v2.4.1). Allele-specific primers were designed using Primer3 web software (<http://frodo.wi.mit.edu/primer3/>). PCR and dideoxy sequencing were performed using standard methods to confirm cosegregation of candidate variants.

## Results

### Clinical findings

#### Family 1

A single affected female (IV-4) was the fourth child born to a consanguineous Pakistani couple (Fig. 1a), reported to have a severe seizure phenotype, poor vision, and profound psychomotor retardation (Table 1). Parents reported an uneventful antenatal, birth and neonatal history, with normal early development. An ocular phenotype of strabismus with nystagmus were the first symptoms described by the parents around 5 months of age. Onset of generalised tonic-clonic (GTC) seizures with excessive startle reflex were observed at 7 months of age with increasing frequency and severity over time, although control was improved after the introduction of phenobarbital. At 1 year of age loss of visual fixation was the earliest sign of regression. Over time further loss of vision, hearing, speech and motor skills progressed with loss of independent sitting and head control and no response to any stimuli by 18 months, associated with

increased GTC seizure frequency. An older male sibling (IV-2) was reported by the parents to have died at the age of 18 months with a similar neurodegenerative phenotype.

#### Family 2

Family 2 comprises five affected individuals (IV-3, IV-4, IV-5, IV-6 and IV-7) with global developmental delay, moderate to severe ID, hypotonia and behavioural problems, including aggression and hyperactivity (Table 1), in a large consanguineous (parents are first-cousins) Pakistani family (Fig. 1d) from Mardan city, a remote region of Khyber Pakhtunkhwa province of Pakistan. Two brothers (IV-3 and IV-4) had infantile focal and multifocal epilepsy with seizure onset at 1.5 and 2.5 years respectively, which has been responsive to antiepileptic medication. Furthermore, three affected individuals (IV-5, IV-6 and IV-7) developed febrile seizures in infancy. All subjects have a below average head size (Table 1), and one individual has microcephaly (IV-3); MRI brain imaging of this individual revealed mild diffuse cerebral atrophy with no sulcal prominence or ventricular enlargement.

#### Family 3

This family comprises two affected siblings (IV-1 and IV-2) with microcephaly, GTC seizures from infancy, moderate to severe ID, global developmental delay, including absent speech, poor memory, and behavioural problems including aggressive episodes and hyperactivity (Table 1), who were born to a consanguineous Pakistani couple (Fig. 1e) from Swat city of the Khyber Pakhtunkhwa province of Pakistan. An EEG performed on individual IV-1 at the age of 3 years showed a mixed background rhythm of beta and theta waves, with abnormal bursts of sharp waves and generalized slow waves on arousal from sedation. MRI brain imaging of this individual (IV-1) shows regions of cortical atrophy, coronal T2 image shows cortical thinning and loss of underlying white matter leading to enlarged fissures in the vermis and cerebellar hemispheres.

### Genetic findings

WES was performed using DNA from a single affected individual (IV-2) from family 1, after filtering variants for quality, zygosity, population frequency and predicted outcome, a single homozygous splice site variant (chr5: g.74689474G > T; c.445 + 1G > T [rs761197472]) was identified in *HEXB* (NM\_000521, a gene previously associated with an autosomal recessive neurodegenerative disorder, for filtering steps in variant prioritization). Dideoxy sequencing confirmed cosegregation of this variant within Family 1 (Fig. 1a, b). This *HEXB* splice variant c.445 + 1G > T is predicted to affect the canonical

**Table 1** Clinical features of families 1, 2 & 3

FAMILY	1			2			3		
	IV-2	IV-4	IV-3	IV-4	IV-5	IV-6	IV-7	IV-1	IV-2
Individual	HEXB HOM c.445 + 1G > T	N/K	MBOAT7 HOM c.758_778del	MBOAT7 HOM c.758_778del	N/K	MBOAT7 HOM c.758_778del	MBOAT7 HOM c.758_778del	MBOAT7 HOM c.758_778del	MBOAT7 HOM c.758_778del
Sex	F	M	M	M	F	F	M	M	F
Age at assessment (years)	20 m	Not assessed (deceased at 18 m)	20	18	16	19	9	8y 1 m	12y
Gestation weeks	FT	N/K	FT	FT	N/K	N/K	FT	FT	FT
Birth weight kg (SD)	3.0 (-0.9)	N/K	3.0 (-1.16)	2.9 (-1.38)	N/K	N/K	2.8	1.5 (-4.6)	1.8 (-3.86)
Height cm (SD)	89 (+ 2.27)	N/K	172.5 (-0.69)	168.8 (-1.2)	N/K	N/K	106.7 (-4.58)	106.7 (-3.93)	127 (-3.2)
Weight kg (SD)	8.5 (-2.67)	N/K	55 (-1.95)	68 (+0.09)	N/K	N/K	30 (+0.34)	N/K	N/K
Head circumference cm (SD)	51 (+ 2.2)	N/K	50 (-2.8)	55.5 (-1.03)	53.6 (-1.25)	55.5 (-0.01)	54 (-1.9)	49 (-3.11)	52 (-1.81)
Development									
Intellectual disability	+	+	Mod-Severe	Severe	Mod-Severe	Mod-Severe	Mod-Severe	Mod-Severe	Mod-Severe
Speech delay/impairment	Non-verbal	+	Non-verbal	Non-verbal	+	+	Non-verbal	Non-verbal	Non-verbal
Developmental delay	+	+	+	+	+	+	+	+	+
Age walking	N/A	N/A	3.5y	4y	N/A	N/A	3.5y	>4y	4y
Neurological features									
Macrocephaly	+	N/K	-	-	-	-	-	-	-
Microcephaly	-	N/K	+	-	-	-	-	+	+
Seizures	Onset 7 m GTCS Regression	+	Onset 1.5y Focal/ multifocal infantile	Onset 2.5y Focal/ multifocal infantile	Febrile seizures in infancy	Febrile seizures in infancy	Febrile seizures in infancy	Onset in infancy GTCS	Onset in infancy GTCS
Hypotonia	+	N/K	+	+	+	+	N/K	+	+
Behavioural problems	N/A	N/A	-	Aggressive episodes	-	-	-	Aggressive episodes Hyperactivity	Aggressive episodes
Other features	Strabismus Nystagmus Visual loss Hearing loss Hepatosplenomegaly	Deceased aged 1.5 years			Unable to walk	Unable to walk			Reduced physical activity level

F female, M male, HOM homozygous, FT full-term, N/A Not applicable, N/K not known, m months, y years, +; feature present, -; feature absent, GTCS generalised tonic-clonic seizure



splicing of exon 2 by abolishing the normal 5' donor splice site, which is predicted to likely result in skipping of exon 2, and possibly promotes the use of a cryptic splice site upstream of the intronic 5' donor sequence (Fig. 1c). This rare variant is present as heterozygous in a single South Asian individual in gnomAD (allele frequency 0.00003266), with no homozygous individuals. A splice variant at the same position (c.445 + 1G > A) has previously been published as a cause of disease in several patients from Argentinian families with SD [13–15] and is reported as pathogenic in ClinVar and the HGMD database. A further splice variant at this position (c.445 + 1G > C) is also listed in ClinVar and dbSNP with conflicting interpretations of pathogenicity.

Genome-wide SNP-array genotyping of DNA from affected individuals IV-3, IV-4 and IV-7 identified a single 1.7 Mb region of shared homozygosity between the affected individuals from rs465169 to rs2112834 (chr19: 54,023,718–55,785,242 [hg38], containing 82 protein coding genes. Of these genes only 9 had OMIM morbid phenotypes: *DNAAF3*, *GP6*, *KIR3DL1*, *MBOAT7*, *NLRP7*, *PRPF31*, *TNNI3*, *TNNT1* and *TSEN34* and only two had associated neurological phenotypes compatible with that of affected individuals within this family: *TSEN34* [16] and *MBOAT7* [7]. *MBOAT7* variant assessment was prioritized as more literature has been reported on the phenotype associated with this gene, including two recently published variants identified within Pakistani families [7] (Table 2). Dideoxy sequencing of *MBOAT7* (NM\_024298.3) using primers that cover both previously identified variants within the Pakistani population (c.820\_826del p.(Gly274Profs\*47) and c.758\_778del; p.(Glu253\_Ala259del)), revealed the 21 base pair in-frame deletion (Chr19:g.54180849\_54180869del21; c.758\_778del; p.(Glu253\_Ala259del) [hg38] [rs750035706]) in exon 6 that cosegregated in family 2 (Fig. 1d, f–g). Due to an overlapping phenotype and common origin of families 2 and 3, we performed dideoxy sequencing for the c.758\_778del *MBOAT7* variant in family 3, which confirmed cosegregation (Fig. 1e). The *MBOAT7* c.758\_778del variant is reported in gnomAD in 5 heterozygous individuals, (four South Asian and one Finnish), with an allele frequency of 0.00002333 (0.0001571 in the South Asian population), and is listed in Clinvar and dbSNP as pathogenic. This variant results in loss of seven highly conserved amino acids (p.Glu253\_Ala259del) [rs750035706] from the *MBOAT7* protein thus producing a shorter protein, and is predicted to be pathogenic by in silico prediction tools. Neither of these identified variants in *HEXB* (c.445 + 1G > T) and *MBOAT7* (c.758\_778del) were present in 65 Pakistani exomes of unaffected individuals.

## Discussion

We investigated three extended consanguineous Pakistani families with individuals affected by undiagnosed childhood onset neurological disease, aiming to provide an accurate molecular diagnosis for these families. WES in a single affected individual in family 1 identified a homozygous splice variant (NM\_000521; c.445 + 1G > T) in *HEXB* that segregated within the family and confirms a diagnosis of SD within this individual and her deceased sibling. The clinical features reported in this patient, including hypotonia, generalized tonic-clonic or myoclonic seizures with regression, blindness, psychomotor retardation, ID, macrocephaly, hepatosplenomegaly, and death in infancy are consistent with previous reports of SD [17, 18]. Many variants have been reported in *HEXB* associated with SD, including 116 pathogenic (DM) variants listed within the Human Gene Mutation Database (HGMDpro, <http://www.hgmd.cf.ac.uk/ac/index.php>). Disruption of the hexosaminidase beta subunit results in a deficiency of the enzymes hexosaminidases A and B, and results in the accumulation of GM2 ganglioside within neurons that results in progressive destruction of the CNS. This is the first description of the c.445 + 1G > T variant that we are aware of within the Pakistani population, although another splice variant at this position (c.445 + 1G > A) has previously been reported in Argentinian families with SD [13, 14].

Genome-wide SNP mapping was carried out using DNA from all three affected individuals from family 2 and identified a 1.7 Mb region of shared homozygosity (chr19: 54,023,718–55,785,242 [hg38]). This region includes the *MBOAT7* gene, recently reported by Johansen et al. (2016) [7] to be associated with a neurodevelopmental phenotype characterised by developmental delay/ID seizures, hypotonia, autistic features and below average head size. This group reported two different homozygous variants in *MBOAT7* within three consanguineous Pakistani families; a 7 bp frameshift deletion (c.820\_826del [p.Gly274Profs\*47]) in exon 6 in four affected individuals from a single family, and an in-frame deletion (c.758\_778del [p.Glu253\_Ala259del]) also in exon 6 in five affected individuals from two unrelated families. We identified the same 21 base pair in-frame deletion (c.758\_778del; p.Glu253\_Ala259del) in families 2 and 3, which cosegregated as appropriate for an autosomal recessive condition. Our findings in these families are consistent with the clinical features described previously (Tables 1 and 3), confirming a diagnosis of an *MBOAT7*-associated disorder in the patients presented here.

This study adds seven affected individuals from two Pakistani families to the literature, with a total of 43 individuals now described with biallelic pathogenic *MBOAT7* variants and similar overlapping phenotypes

**Table 2** MBOAT7 variants published to date associated with autosomal recessive neurodevelopmental disorder

Publications	Number of individuals	Number of families	Origin	Transcript	gDNA position [hg38]	cDNA position	Predicted Protein change	Exon	Type	gnomAD frequency (All)
Present paper	7	2	Pakistan	NM_0242983	g.54180849_54180869del21	c.758_778del	p.Glu253_Ala259del	6	Inframe deletion	0.00002333
Johansen et al (2016)	5	2	Pakistan	NM_0242983	g.54180849_54180869del21	c.758_778del	p.Glu253_Ala259del	6	Inframe deletion	0.00002333
Johansen et al (2016) [7]	4	1	Pakistan	NM_0242983	g.54180801_54180807delGGCCGCC	c.820_826del	p.Gly274Profs*47	6	Frameshift	-
Johansen et al (2016) [7]	3	1	Egypt	NM_0242983	g.54188278_54188297del20	c.126_145del	p.Leu43Hisfs*69	3	Frameshift	-
Johansen et al (2016) [7]	2	1	Jordan	NM_0242983	g.54183591delC	c.423delG	p.Leu142Cysfs*8	5	Frameshift	-
Johansen et al (2016) [7]	2	1	Iraq	NM_0242983	g.54180772C > G	c.854 + 1G > C	p.?	Intron	Splice	-
Hu et al (2018) [9]	3	1	Iran	NM_0242983	g.54174394C > T	c.1069G > A	p.Gly357Ser	8	Missense	0.00001702
Santos-Cortez et al (2018) [8]	4	1	Pakistan	NM_0242983	g.54187242delA	c.251delT	p.Leu84AArgfs*25	8	Frameshift	-
Yalinizoglu et al (2019) [6]	3	1	Turkey	NM_0242983	g.54174186G > A	c.1278G > A	p.Trp426*	8	Nonsense	-
Yalinizoglu et al (2019) [6]	4	2	Turkey	NM_0242983	g.54162440_54174072del	c.?	p.?	8	Deletion	-
Yalinizoglu et al (2019) [6]	2	1	Turkey	NM_0242983	g.54187234C > T	c.259C > T	p.Arg87Gln	4	Missense	0.00001108
Yalinizoglu et al (2019) [6]	2	2	Turkey	NM_0242983	g.54180936_54180946del	c.680_690del	p.Leu227Profs*65	6	Frameshift	0.000004919
Yalinizoglu et al (2019) [6]	1	1	Turkey	NM_0242983	g.54174337C > T	c.1126G > A	p.Glu376Lys	8	Missense	0.00003211
Jacher et al. (2019) [10]	1	1	Lebanon	NM_0242983	g.54178943 T > C	c.855-2A > G	p.?	Intron	Splice	-



**Table 3** Clinical features of all published cases associated with biallelic *MBOAT7* variants

Publications	Current study	Johansen et al [7]	Hu et al [9]	Santos-Cortez et al [8]	Yalnizoglu et al [6]	Jacher et al [10]	Total (n = 39)
Sex	M = 4, F = 3	M = 7, F = 9	M = 3, F = 0	M = 2, F = 2	M = 5, F = 7	M = 0, F = 1	M = 21, F = 22
Consanguinity	7/7 (100%)	16/16 (100%)	3/3 (100%)	4/4 (100%)	12/12 (100%)	0/1 (0%)	42/43 (98%)
Development							
Developmental delay	7/7 (100%)	16/16 (100%)	0/3 (0%)	4/4 (100%)	12/12 (100%)	1/1 (100%)	40/43 (93%)
Speech delay	7/7 (100%)	16/16 (100%)	0/3 (0%)	4/4 (100%)	12/12 (100%)	1/1 (100%)	40/43 (93%)
Non-verbal	5/7 (71%)	9/16 (56%)	0/3 (0%)	N/K	N/K	0/1 (0%)	14/27 (52%)
Single words	2/7 (29%)	7/16 (44%)	N/K	N/K	N/K	1/1 (100%)	10/24 (42%)
Two word sentences	0/7 (0%)	2/16 (13%)	N/K	N/K	3/12 (25%)	1/1 (100%)	6/36 (17%)
Motor delay	7/7 (100%)	16/16 (100%)	0/3 (0%)	N/K	12/12 (100%)	1/1 (100%)	36/39 (92%)
Never walked	0/7 (0%)	3/16 (19%)	0/3 (0%)	N/K	0/12 (0%)	0/1 (0%)	3/39 (8%)
Neurological features							
Intellectual disability	7/7 (100%)	16/16 (100%)	3/3 (100%)	4/4 (100%)	12/12 (100%)	1/1 (100%)	43/43 (100%)
Lower than average OFC	7/7 (100%)	16/16 (100%)	0/3 (0%)	4/4 (100%)	N/K	0/1 (0%)	27/31 (87%)
Microcephaly	2/7 (29%)	6/16 (38%)	0/3 (0%)	2/4 (50%)	N/K	0/1 (0%)	10/31 (32%)
Macrocephaly	0/7 (0%)	0/16 (0%)	0/3 (0%)	0/4 (0%)	0/7 (0%)	1/1 (100%)	1/43 (2%)
Seizures	6/7 (86%)	10/16 (63%)	3/3 (100%)	N/K	11/12 (92%)	1/1 (100%)	31/39 (79%)
Generalised tonic clonic	0/7 (0%)	1/16 (6%)	N/K	N/K	2/12 (17%)	0/1 (0%)	3/36 (8%)
Myoclonic/infantile spasm	0/7 (0%)	5/16 (31%)	N/K	N/K	3/12 (25%)	0/1 (0%)	8/36 (22%)
Focal	2/7 (29%)	2/16 (13%)	N/K	N/K	1/12 (8%)	1/1 (100%)	6/36 (17%)
Febrile seizures	2/7 (29%)	2/16 (13%)	N/K	N/K	1/12 (8%)	0/1 (0%)	5/36 (14%)
Hypotonia	6/7 (86%)	15/16 (94%)	N/K	N/K	12/12 (100%)	1/1 (100%)	34/36 (94%)
Hypertonia	0/7 (0%)	16/16 (100%)	N/K	N/K	0/12 (0%)	0/1 (0%)	16/36 (44%)
Behavioural problems/ASD	3/7 (43%)	7/16 (44%)	3/3 (100%)	N/K	4/12 (33%)	1/1 (100%)	18/39 (46%)
Poor coordination/ataxic gait	0/7 (0%)	0/16 (0%)	N/K	N/K	11/12 (92%)	N/K	11/35 (31%)
Neuroimaging							
Polymicrogyria	1/7 (14%)	6/16 (38%)	1/3 (33%)	N/K	12/12 (100%)	1/1 (100%)	21/39 (54%)
Cortical atrophy	0/1 (0%)	2/6 (13%)	0/3 (0%)	N/K	0/12 (0%)	0/1 (0%)	2/23 (9%)
Cerebellar dysgenesis	1/1 (100%)	2/6 (13%)	0/3 (0%)	N/K	8/12 (67%)	0/1 (0%)	11/23 (45%)
Leukoencephalopathy	0/1 (0%)	0/6 (0%)	0/3 (0%)	N/K	8/12 (67%)	0/1 (0%)	8/23 (35%)
Other features							
Strabismus	N/K	N/K	1/3 (33%)	N/K	5/12 (42%)	1/1 (100%)	7/16 (44%)
Retinal/macular degeneration	0/12 (0%)	N/K	2/3 (67%)	N/K	N/K	0/1 (0%)	2/16 (13%)
Optic atrophy	0/12 (0%)	N/K	3/3 (100%)	N/K	N/K	0/1 (0%)	3/16 (19%)
Hyperphagia/obesity	0/12 (0%)	N/K	3/3 (100%)	N/K	N/K	1/1 (100%)	4/16 (25%)
Short stature	3/7 (43%)	N/K	0/3 (0%)	N/K	N/K	0/1 (0%)	3/11 (27%)

Comparison of clinical features of all published cases of neurological disorder associated with biallelic *MBOAT7* variants, showing number and percentage of individuals (in brackets) with each feature. OFC occipitofrontal circumference, ASD autistic spectrum disorder, N/K not known

(Table 3). A total of 13 *MBOAT7* variants associated with autosomal recessive neurodevelopmental disorder have been described to date (Table 2); nine of which are truncating and loss-of-function variants and not tolerated in gene constraint predictions with a pLI score of

0.113 in gnomAD. A total of 12 individuals from four consanguineous Pakistani families with a similar neurodevelopmental phenotype have now been reported as homozygous for the *MBOAT7* c.758\_778del variant (Table 2). The further two families reported here

contribute to knowledge of the phenotypical spectrum of neurological disorder associated with disruption of *MBOAT7*, characterised by the universal feature of moderate to severe ID, usually associated with significant global developmental delay, profound speech impairment (52% are non-verbal), motor delay (8% never walk) and lower than average OFC (32% have microcephaly) (Table 3). Other frequent features are seizures in 79%, including GTC, myoclonic, infantile spasm, focal and multifocal seizures, hypotonia is reported in 94% (often described as truncal hypotonia in infancy), hypertonia is also reported in 44%, autistic features and behavioral problems include aggressive episodes, hyperactivity, stereotypies (rocking and hand flapping) in 46%. Jacher et al. [10] reported macrocephaly with overgrowth in a single patient, although macrocephaly has not been observed in any other previously reported cases. While we cannot exclude additional genetic or environmental causes our data suggest that short stature (below  $-3$  SD identified in 3/5 individuals) may also be a feature of *MBOAT7*-related disorder. MRI imaging identified several common findings of cortical atrophy in 45%, cerebellar dysgenesis in 35%, leukoencephalopathy in 10% and polymicrogyria in 9% of individuals who underwent imaging and as previously discussed by Yalnizoglu et al [6], these findings are common to other complex lipid biosynthesis and remodeling disorders.

The *MBOAT7* gene encodes LPIAT1, an enzyme present in endomembranes that contributes to the regulation of free arachidonic acid (AA) in the cell through the remodeling of phospholipids via the Land's cycle [19, 20]. Lee et al. [18] discovered that LPIAT1 is required for cortical lamination in *Mboat7*<sup>-/-</sup> mice and brain histology of these mice showed a smaller cerebral cortex, with increased apoptotic cells and increased gyral structures. These findings are comparable with the phenotype observed in humans of cortical atrophy, reduced head size and polymicrogyria. Interestingly, *Mboat7*<sup>-/-</sup> mice show significantly smaller stature than their wildtype littermates [21], and is a feature that we have identified in our patient cohort with 3/5 individuals with height  $< -3$  SD below the mean, confirming this as a novel feature associated with *MBOAT7*-related neurodevelopmental disorder.

## Conclusions

Interestingly both protein products of *MBOAT7* and *HEXB* genes are involved in metabolic disorders of lipid biosynthesis and remodeling within the brain, and this group of disorders are an important and often overlooked consideration in the differential diagnosis of neurodevelopmental disorders [22]. Investigation and identification of the genetic basis of neurodevelopmental disorders identified within the three Pakistani families

reported here provide us with a better understanding of the spectrum of neurological disease and responsible gene variants present within this population to aid diagnosis in other families who may be affected by these conditions. Accurate molecular disease diagnosis allows a specific diagnosis to be provided to families and their clinicians to provide targeted management strategies, appropriate genetic counselling, improved carrier detection and the possibility of prenatal testing where available. Our findings highlight the *MBOAT7* c.758\_778del variant as a cause of developmental delay/ID in the Pakistani population, and broaden knowledge of the phenotypical outcomes associated with *MBOAT7* gene variants.

## Abbreviations

AA: Arachidonic acid; ExAC: Exome Aggregation Consortium; GM2: Gangliosidases; GnomAD: Genome Aggregation Data base; GTCs: Generalized tonic clonic seizure; *HEXA*: Hexosaminidase A; *HEXB*: Hexosaminidase B; HGMD: Human gene mutation data base; HOM: Homozygous; ID: Intellectual disability; LPIAT1: Lysophosphatidyl inositol acetyl transferase 1; *MBOAT7*: Membrane bound O-acyltransferase family member 7; MRI: Magnetic Resonance Imaging; SD: Sandhoff disease; SNP: Single Nucleotide Polymorphism; WES: Whole Exome Sequencing

## Acknowledgments

The authors would like to thank the Pakistani families for their participation in the research study.

## Author's contributions

SK, AU, and MJ recruited families and collected/compiled clinical information with help of LER, ELB and AHC. SK, GVH, and MU, performed genetic studies, and analyzed data alongside GVH, AHC, WA, LER, AG, AU, ELB, Manuscript writing and revision: SK, LER, GVH, MU, SS, ELB, AHC, AH and AG. Study supervision and coordination: ELB, AHC, and AG. The final version of the manuscript was read and approved by all authors.

## Funding

Shazia Khan was supported by International Research Support Initiative Program (IRSIP) from HEC, Islamabad, Pakistan. The funding body played no role in the design of the study and collection, analysis, and interpretation of data and in writing the manuscript.

## Availability of data and materials

The datasets used and/or analysed during the current study are available from the corresponding author on reasonable request.

## Ethics approval and consent to participate

The study was approved by the Institutional Review Boards of International Islamic University, Islamabad, Pakistan and University of Exeter, UK, in accordance with Declaration of Helsinki protocols. Written informed consent to participate was obtained from all individuals (or those with parental responsibility).

## Consent for publication

Written informed consent for publication of research findings was obtained from all individuals (or those with parental responsibility) who participated in the study.

## Competing interests

Wasim Ahmad is a member of the editorial board (Associate Editor) of *BMC Medical Genetics*. The remaining authors declare that they have no competing interests.

## Author details

<sup>1</sup>Department of Biological Sciences, International Islamic University Islamabad, H-10, Islamabad 44000, Pakistan. <sup>2</sup>Medical Research, RILD Wellcome Wolfson Centre (Level 4), Royal Devon and Exeter NHS Foundation

Trust, Exeter, Devon EX2 5DW, UK. <sup>3</sup>Department of Biochemistry, Faculty of Biological Sciences, Quaid-i-Azam University, Islamabad, Pakistan. <sup>4</sup>Peninsula Clinical Genetics Service, Royal Devon & Exeter Hospital (Heavitree), Gladstone Road, Exeter EX1 2ED, UK. <sup>5</sup>Rajarshi Shahu College of Pharmacy, Malvihiir Buldana, Maharashtra, Buldana 443001, India. <sup>6</sup>Medical Genomics Research Department, King Abdullah International Medical Research Center (KAIMRC), King Saud bin Abdulaziz University for Health Sciences, Ministry of National Guard–Health Affairs (MNGHA), P.O. Box 3660, Riyadh 11481, Kingdom of Saudi Arabia. <sup>7</sup>Department of Molecular Biology, Shaheed Zulfiqar Ali Bhutto Medical University, Islamabad, Pakistan. <sup>8</sup>National Institute for Genomics & Advanced Biotechnology, NARC, Islamabad 45500, Pakistan.

Received: 22 May 2019 Accepted: 15 October 2019

Published online: 18 December 2019

## References

- Durkin MS, Hasan ZM, Hasan KZ. Prevalence and correlates of mental retardation among children in Karachi, Pakistan. *Am J Epidemiol*. 1998; 147(3):281–8.
- Khatri IA, Iannaccone ST, Ilyas MS, Abdullah M, Saleem S. Epidemiology of epilepsy in Pakistan: review of literature. *J Pak Med Assoc*. 2003;53(12):594–7.
- Ahmad F, Bilal M, Khan A, Umair M. Genetic skeletal disorders in Pakistan: A brief commentary. *Meta Gene*. 2019;20:100559. <https://doi.org/10.1016/j.mgene.2019.100559>.
- Sandhoff K, Andreae U, Jatzkewitz H. Deficient hexosaminidase activity in an exceptional case of Tay-Sachs disease with additional storage of kidney globoside in visceral organs. *Pathol Eur*. 1968;3(2):278–85.
- Hendriks CJ, Corry PC, Wraith JE, Besley GT, Cooper A, Ferrie CD. Juvenile Sandhoff disease—nine new cases and a review of the literature. *J Inher Metab Dis*. 2004;27(2):241–9.
- Yalnızoğlu D, Özgül RK, Oğuz KÇ, Özer B, Yücel-Yılmaz D, Gürbüz B, et al. Expanding the phenotype of phospholipid remodelling disease due to MBOAT7 gene defect. *J Inher Metab Dis*. 2019;42(2):381–8.
- Johansen A, Rosti RO, Musaev D, Sticca E, Harripaul R, Zaki M, et al. Mutations in MBOAT7, encoding Lysophosphatidylinositol Acyltransferase I, Lead to intellectual disability accompanied by epilepsy and autistic features. *Am J Hum Genet*. 2016;99(4):912–6.
- Santos-Cortez RLP, Khan V, Khan FS, Mughal ZU, Chakchouk I, Lee K, et al. Novel candidate genes and variants underlying autosomal recessive neurodevelopmental disorders with intellectual disability. *Hum Genet*. 2018; 137(9):735–52.
- Hu H, Kahrizi K, Musante L, Fattahi Z, Herwig R, Hosseini M, et al. Genetics of intellectual disability in consanguineous families. *Mol Psychiatry*. 2019;24(7): 1027–1039. <https://doi.org/10.1038/s41380-017-0012-2>. Epub 2018 Jan 4.
- Jacher JE, Roy N, Ghaziuddin M, Innis JW. Expanding the phenotypic spectrum of MBOAT7-related intellectual disability. *Am J Med Genet B Neuropsychiatr Genet*. 2019;180(7):483–487. <https://doi.org/10.1002/ajmg.b.32749>. Epub 2019 Jul 8.
- Lee HC, Inoue T, Imae R, Kono N, Shirae S, Matsuda S, et al. *Caenorhabditis elegans* mboa-7, a member of the MBOAT family, is required for selective incorporation of polyunsaturated fatty acids into phosphatidylinositol. *Mol Biol Cell*. 2008;19(3):1174–84.
- Dauwerse JG, de Vries BB, Wouters CH, Bakker E, Rappold G, Mortier GR, et al. A t(4;6)(q12;p23) translocation disrupts a membrane-associated O-acetyl transferase gene (MBOAT1) in a patient with a novel brachydactyly-syndactyly syndrome. *Eur J Hum Genet*. 2007;15(7):743–51.
- Kleiman FE, de Kremer RD, de Ramirez AO, Gravel RA, Argaraña CE. Sandhoff disease in Argentina: high frequency of a splice site mutation in the HEXB gene and correlation between enzyme and DNA-based tests for heterozygote detection. *Hum Genet*. 1994;94(3):279–82.
- Brown CA, McInnes B, de Kremer RD, Mahuran DJ. Characterization of two HEXB gene mutations in Argentinean patients with Sandhoff disease. *Biochim Biophys Acta*. 1992;1180(1):91–8.
- Zampieri S, Cattarossi S, Oller Ramirez AM, Rosano C, Lourenco CM, Passon N, et al. Sequence and copy number analyses of HEXB gene in patients affected by Sandhoff disease: functional characterization of 9 novel sequence variants. *PLoS One*. 2012;7(7):e41516.
- Budde BS, Namavar Y, Barth PG, Poll-The BT, Nürnberg G, Becker C, et al. tRNA splicing endonuclease mutations cause pontocerebellar hypoplasia. *Nat Genet*. 2008;40(9):1113–8.
- Sung AR, Moretti P, Shaibani A. Case of late-onset Sandhoff disease due to a novel mutation in the. *Neurol Genet*. 2018;4(4):e260.
- Gaignard P, Fagart J, Niemir N, Puech JP, Azougouene E, Dussau J, et al. Characterization of seven novel mutations on the HEXB gene in French Sandhoff patients. *Gene*. 2013;512(2):521–6.
- Pérez-Chacón G, Astudillo AM, Balgoma D, Balboa MA, Balsinde J. Control of free arachidonic acid levels by phospholipases A2 and lysophospholipid acyltransferases. *Biochim Biophys Acta*. 2009;1791(12):1103–13.
- Caddeo A, Jamialahmadi O, Solinas G, Pujia A, Mancina RM, Pingitore P, et al. MBOAT7 is anchored to endomembranes by six transmembrane domains. *J Struct Biol*. 2019;206(3):349–60. <https://doi.org/10.1016/j.jsb.2019.04.006>.
- Lee HC, Inoue T, Sasaki J, Kubo T, Matsuda S, Nakasaki Y, et al. LPIAT1 regulates arachidonic acid content in phosphatidylinositol and is required for cortical lamination in mice. *Mol Biol Cell*. 2012;23(24):4689–700.
- García-Cazorla A, Mochel F, Lamari F, Saudubray JM. The clinical spectrum of inherited diseases involved in the synthesis and remodeling of complex lipids. A tentative overview. *J Inher Metab Dis*. 2015;38(1):19–40.

## Publisher's Note

Springer Nature remains neutral with regard to jurisdictional claims in published maps and institutional affiliations.

**Ready to submit your research? Choose BMC and benefit from:**

- fast, convenient online submission
- thorough peer review by experienced researchers in your field
- rapid publication on acceptance
- support for research data, including large and complex data types
- gold Open Access which fosters wider collaboration and increased citations
- maximum visibility for your research: over 100M website views per year

**At BMC, research is always in progress.**

Learn more [biomedcentral.com/submissions](https://biomedcentral.com/submissions)




RESEARCH ARTICLE

Open Access



# Novel nonsense variants in *SLURP1* and *DSG1* cause palmoplantar keratoderma in Pakistani families

Abida Akbar<sup>1,2</sup>, Claire Prince<sup>2</sup>, Chloe Payne<sup>2</sup>, James Fasham<sup>2</sup>, Wasim Ahmad<sup>3</sup>, Emma L. Baple<sup>2</sup>, Andrew H. Crosby<sup>2</sup>, Gaurav V. Harlalka<sup>2,4</sup> and Asma Gul<sup>1\*</sup> 

## Abstract

**Background:** Inherited palmoplantar keratodermas (PPKs) are clinically and genetically heterogeneous and phenotypically diverse group of genodermatoses characterized by hyperkeratosis of the palms and soles. More than 20 genes have been reported to be associated with PPKs including desmoglein 1 (*DSG1*) a key molecular component for epidermal adhesion and differentiation. Mal de Meleda (MDM) is a rare inherited autosomal recessive genodermatosis characterized by transgrediens PPK, associated with mutations in the secreted LY6/PLAUR domain containing 1 (*SLURP1*) gene.

**Methods:** This study describes clinical as well as genetic whole exome sequencing (WES) and di-deoxy sequencing investigations in two Pakistani families with a total of 12 individuals affected by PPK.

**Results:** WES identified a novel homozygous nonsense variant in *SLURP1*, and a novel heterozygous nonsense variant in *DSG1*, as likely causes of the conditions in each family.

**Conclusions:** This study expands knowledge regarding the molecular basis of PPK, providing important information to aid clinical management in families with PPK from Pakistan.

**Keywords:** Mal de Meleda, Palmoplantar keratoderma, *SLURP1*, *DSG1*, Mutation, Variant, Exome sequencing

## Background

Palmoplantar keratoderma (PPK) is a heterogeneous entity of both genetics and acquired keratinization disorder, which is characterized by persistent marked epidermal thickening of palms and soles [1]. Hereditary PPKs comprising an increasing number of entities with different prognoses, which may be associate with cutaneous and extracutaneous manifestations [2].

Depending on different patterns of hyperkeratosis, PPKs are further classified into four distinct types: diffuse, striate, focal and punctate [3, 4]. So far, deleterious mutations in > 20 genes have been reported in pathogenesis of different forms of hereditary PPKs [3, 4]. In last few years, advent of cutting edge genetic techniques such as whole genome microarray scans and whole exome sequencing

have incredibly accelerated the identification of disease causing variants in many genes involved in various inherited forms of PPKs, and thus significantly increasing understanding about intricate molecular mechanisms of heterogeneous disorders, consecutively aiding valuable genetic counselling and patient care [3].

Mal de Meleda (MDM), a type of transgradient palmoplantar keratoderma (PPK), is a rare autosomal recessive disorder. Luca Stulli, a Croatian born scientist in 1826 first described Mal de Meleda on the Adriatic Meleda island (now Mljet) [5]. The disease can feature other potentially disfiguring effects on the hands and feet that can severely impact function.

The disease onset is soon after birth and is clinically characterized by erythema, transgradients and progradients hyperkeratosis of palms and soles with well demarcated borders and hypohydrosis. Other associated features are brachydactyly, nail abnormalities and lichenoid plaques [6]. Rigorous keratoderma can lead to deformity in

\* Correspondence: [gulasma@iiu.edu.pk](mailto:gulasma@iiu.edu.pk)

<sup>1</sup>Department of Biological Sciences, International Islamic University, H-10, Islamabad 44000, Pakistan

Full list of author information is available at the end of the article



hands and feet and gradually this may result into severe impairment [7, 8].

Furthermore, previous reports have shown that MDM may be caused due to mutations in the *SLURPI* gene (previously known as ARS-B gene) encoding a secreted toxin-like mammalian lymphocyte antigen 6/urokinase-type plasminogen activator receptor-related protein 1 (*SLURPI*). Expression of *SLURPI* is reported in epithelium, stomach, sensory nerve cells, gums, esophagus and immune cells with highest level in keratinocytes especially in palms and soles [9–11].

Striate PPK type I is a rare type of PPK and shows the autosomal dominant mode of inheritance associated with *DSG1* heterozygous mutation. Clinical features of this condition are linear hyperkeratotic lesions on the palms extending along the length of fingers and associated with thick patches of diffuse hyperkeratosis on the soles [12].

Heterozygous mutation in *DSG1* gene in an autosomal dominant pattern have also been reported in focal PPK in a Libyan family, and in a Jewish Yemenite family with diffuse PPK [13, 14], a discovery which elucidates that different patterns of palmoplantar involvement may result from mutations in the *DSG1* gene. Additionally, bi-allelic mutations in *DSG1* gene have also been recently reported in the severe SAM syndrome, characterized by sinusitis, palmoplantar keratoderma, erythroderma, multiple allergies and metabolic defects, with heterozygous mutation carriers only presenting hyperkeratotic palmoplantar lesions [15].

Here we report findings regarding investigations of two families from Pakistan with clinically-defined PPK, for which the specific genetic basis was unclear.

## Methods

### Genetic studies

The research work presented in this manuscript was approved by the Ethical Review Boards Committee at International Islamic University, Islamabad, Pakistan (IIUI; Pakistan). Informed written consent was obtained for all participants for the collection of blood samples, with clinical evaluations and family histories performed by a dermatologist. Extraction of high quality genomic DNA from the whole blood was carried out by using the ReliaPrep™ kit (Blood gDNA Miniprep System, Promega) following the manufacturer's protocol. Whole exome sequencing (WES) was undertaken on a NextSeq500 (Illumina, CA, San Diego, USA) with targeting using Agilent Sure select Whole Exome v6. The reads were aligned using BWA-MEM (v0.7.12), with mate-pairs fixed and duplicates removed using Picard (v1.129). InDel realignment and base quality recalibration were performed using GATK (v3.4–46). SNVs and InDels were detected using GATK Haplotype Caller or SnpEff tool ([http://snpeff.sourceforge.net/SnpEff\\_manual.html](http://snpeff.sourceforge.net/SnpEff_manual.html)), and annotated using Alamut batch (v1.4.4). Read depth was determined for the whole exome using GATK Depth of Coverage.

Primer3 web software was used to design the allele-specific primers (primer sequences are available upon request) to validate and verify the segregation of identified variants via Sanger sequencing. Polymerase chain reaction (PCR) was performed for all affected and healthy individuals of recruited families by using allele-specific primers following standard conditions, with products sequenced by Source Bio-Science Life Sciences (<https://www.sourcebioscience.com/>).

## Results

### Subjects

Pedigree analysis was indicative of an autosomal recessive inheritance pattern of family 1, and an autosomal dominant mode of inheritance of family 2 (Fig. 1). All 12 living affected individuals with PPK as well as 6 unaffected (healthy) individuals including parents and siblings from both families (Family 1 and 2) were investigated. The seven affected individuals from family 1: IV:7, IV:8, IV:12, V:2, V:4, V:8 and V:9 were 27, 22, 45, 16, 11, 15 and 13 years of age respectively at the time of examination, while the five affected individuals from family 2: III:2, III:5, III:6, IV:1 and IV:2 were 28, 36, 40, 12 and 8 years of age respectively. On the basis of basic clinical dermatological examination, PPK was the main finding exhibit in all patients (affected members) of the recruited families.

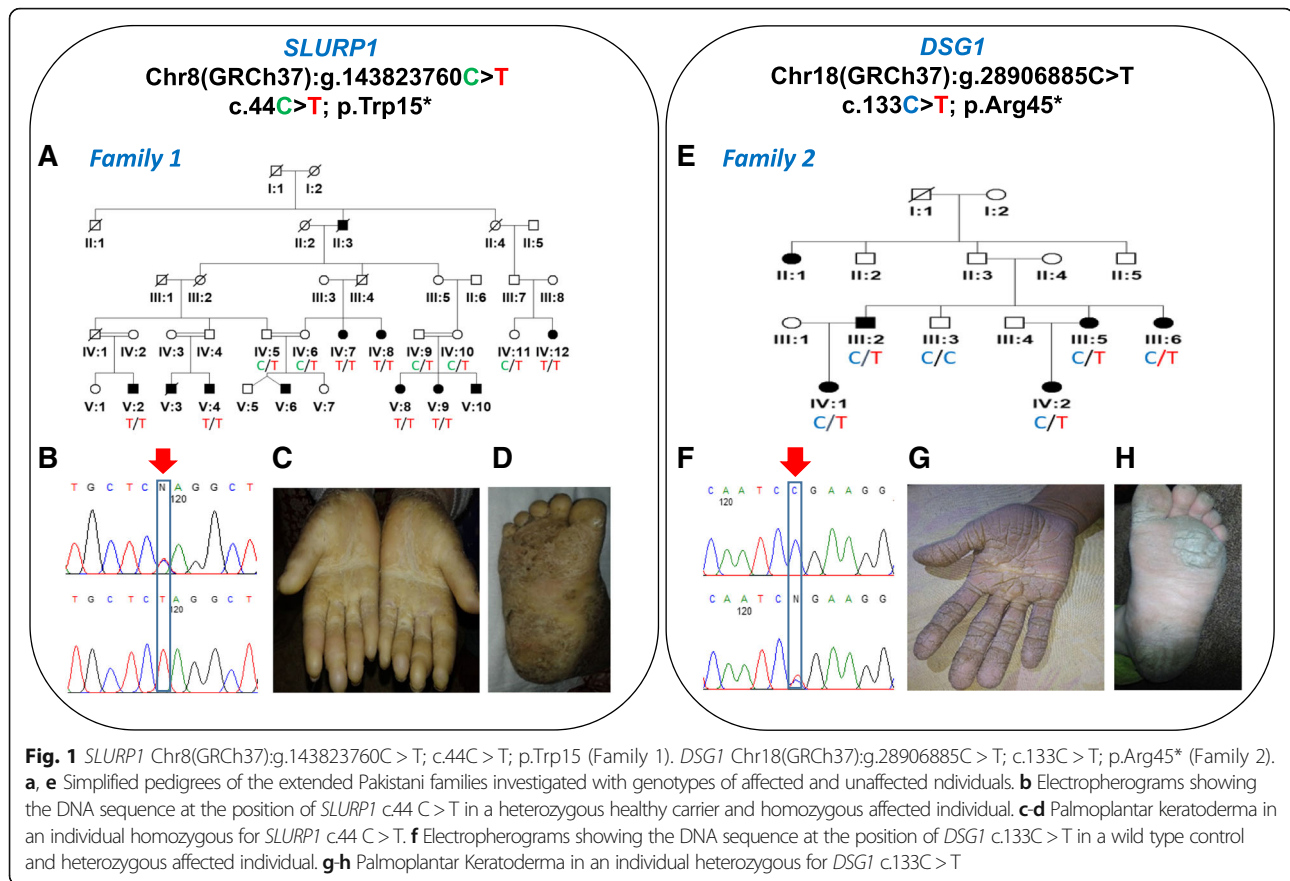
Disease onset was from 3 months to 1 year. Affected individuals of family 1 show cuff-like pattern with well demarcated margins and waxy yellow tone on hands and feet. Diffuse hyperkeratosis of hand and feet was common in patients. Fingers were tapered towards the tips and flexion deformity due to contractures was observed in 2 (IV:7 and IV:8) patients. Knuckle pads were observed in interphalangeal joints and hyperhidrosis was also common in all patients. Patients in family 2 showed diffuse hyperkeratosis with cracks and fissuring of the volar surface of the digits of hands and soles, toes were observed in two siblings. All other patients have mild hyperkeratosis. Mild to severe deafness was observed in patients and one patient (III:5) was deaf as well as mute. Both families' phenotypes are summarized in Table 1 and Fig. 1.

All patients of family 1 and 2 were intellectually normal and hair, nail, teeth and cardiac anomalies were not observed in any of the patient. Disease conditions worsened due to aging.

### Genetic findings

To identify the causative gene mutation, single affected individual from each of the family was initially selected





to perform WES (subject IV:12 of family 1 and III:2 of family 2, Fig. 1) to generate a profile of rare and novel sequence variants, with regard to mode of inheritance in each of the families. After that, exome data was first reviewed to identify pathogenic variants in disease associated genes, filtering for highly likely deleterious (nonsense, frame-shift, non-synonymous exonic or splice-site) variants for comparison with allele frequencies in online genome databases (including the Exome Aggregation Consortium; ExAC, the 1000 Genomes Project and the Genome Aggregation Database; gnomAD). This identified a single candidate novel homozygous nonsense variant [NM\_020427.2:c.44G > A; Chr8:143823760C > T (GRCh37)] in the first coding exon of *SLURP1* gene (Fig. 1) in family 1. This variant leads to substitution of tryptophan by a premature termination codon and is at the evolutionary conserved position 15 (p.Trp15\*). In family 2, a heterozygous variant [NM\_001942.3:c.133C > T; Chr18:28906885C > T (GRCh37)] was identified in coding exon 3 of the *DSG1* gene (Fig. 1), which is predicted to result in a premature stop codon (p.Arg45\*). The *SLURP1* gene variant in family 1 is not listed in online genome databases and segregates as predicted for an autosomal recessive form in family 1. The *DSG1* gene variant identified of family 2 is listed in the gnomAD

browser database in 1 Latino individual in heterozygous form out of 31,370 genomes, corresponding to a minor allele frequency of 0.00003188; both variants are summarized in Additional file 1: Tables S1 and S2 alongside all other reported disease-associated *SLURP1* and *DSG1* variants.

## Discussion

*SLURP1* has been localized to the granular layer of epidermis [16], where it functions as part of nicotinic acetylcholine receptors found on keratinocyte cells as a pro-apoptotic protein [17]. Arredondo et al. [17] demonstrated that keratinocytes are stimulated by *SLURP1* through nicotinic acetylcholine receptor, leading to decline in keratinocytes cell number, indicative of the inhibitory and regulatory nature of *SLURP1*. Therefore, when *SLURP1* is non-functional, as seen in Mal de Meleda, severe hyperkeratosis results due to improper keratinocyte apoptosis regulation [8, 18].

We identified nonsense variant in family 1 which causes substitution of evolutionarily conserved tryptophan at 15th amino acid position in *SLURP1* by a premature termination codon. Nonsense variant (c.129C > A; p.Cys43\*) is also reported in exon 2 of *SLURP1* gene in a Turkish



**Table 1** Clinical phenotypes of study participants of family 1 and 2

Individuals	Family 1							Family 2				
	IV:7	IV:8	IV:12	V:2	V:4	V:8	V:9	III:2	III:5	III:6	IV:1	IV:2
Age	27 years	22 years	45 Years	16 years	11 years	15 years	13 years	28 years	36 years	40 years	12 years	8 years
Sex	F	F	F	M	M	F	F	M	F	F	F	F
Disease onset	1 year	1 year	6 months	6 months	1 year	3 months	6 months	By birth	By birth	By birth	By birth	By birth
Inheritance	Autosomal Recessive							Autosomal Dominant				
Diffuse PPK	+	+	+	+	+	+	+	+	+	+	+	+
Scale colour	Yellowish	Yellowish	Yellowish	Yellowish	Yellowish	Yellowish	Yellowish	-	-	-	-	-
Cuff like margins	++	++	++	++	++	++	++	-	-	-	-	-
Pseudoainhum	-	-	-	-	-	-	-	-	-	-	-	-
Cracked Hyperkeratosis	-	-	-	-	-	-	-	++	+++	+	+	+
Deafness	-	-	-	-	-	-	-	Mild	Complete	Mild	Mild	Mild
Speech abnormality	-	-	-	-	-	-	-	Mild	Complete	-	-	-
Diffuse hyperkeratosis	-	-	-	-	-	-	-	Severe	Severe	Mild	Mild	Mild
Teeth, hairs and nails	Normal	Normal	Normal	Normal	Normal	Normal	Normal	Normal	Normal	Normal	Normal	Normal
Finger deformity	-	++	++	+	-	-	-	-	+	+	-	-
Hyperhidrosis	+	+	+	+	+	+	+	-	-	-	-	-
Cardiomyopathy	-	-	-	-	-	-	-	-	-	-	-	-

+ = presence of feature, - = absence of feature, +++ = present in severe form

family. Similarly another nonsense mutation (c.286C > T; p.Arg96\*) is also found in exon 3 in Croatian family and is predicted to truncate protein synthesis via nonsense-mediated mRNA decay [19, 20]. Family reported in this study have same clinical features to previously reported Mal de Meleda families.

The *SLURP1* gene mutation p.Gly86Arg is most often found in sporadic patients with MDM of Asian origin [21, 22].

So far 20 mutations in *SLURP1* are reported to cause Mal de Meleda, a form of PPK (Additional file 1: Table S1). c.44G > A; p.Trp15Term is the second variant identified in Pakistan apart from c.2 T > C, p.Met1Thr variant which was recently reported [23].

“Desmoglein” comprises of the two Greek words “desmos” for “tie” and “glein” for “glue-like.” Perturbations of desmoglein expression in the epidermis have been known to impact cell adhesion properties. *DSG1* is distinctively located, just above the stratum germinativum, to be candidate of epidermis stratification and differentiation [24]. A study in which *DSG1* was down regulated in skin culture confirmed the importance of *DSG1* for directing those functions [25].

In all reported PPKs cases where *DSG1* gene variants (frameshift or nonsense) have been reported, there is evidence that affected protein haploinsufficiency leads to the striate, focal PPK and striate PPK with wooly hair

and cardiomyopathy. Haploinsufficiency is predicted to cause through nonsense mediated mRNA decay because of premature termination codons [26, 27]. Interestingly, a heterozygous *DSG1* mutation has also been reported in focal PPK [13].

To date, 31 mutations (8 nonsense mutations, 14 frame-shift variants and 9 splice-site variants) in *DSG1* have been reported to cause striate/focal PPK (Additional file 1: Table S2). In 2009, Dua-Awereh et al. reported five heterozygous variants (p.Arg26\*; c.373-2A > G; c.515C > T; c.1266-3C > G and c.1399delA) in *DSG1* gene in five families with autosomal dominant striate PPK [28]. Thus, c.133C > T; p.Arg45\* variant identified in this study is the sixth mutation underlying dominantly inherited form of striate PPK in Pakistan.

MDM presented a consistently severe phenotype than Nagashima form of PPK. MDM shows progressive hyperkeratosis among all PPKs and causes flexion contracture and constricting band [29]. While, Nagashima PPK is characterized by non-progressive and mild hyperkeratosis and does not show flexion contracture and constricting band [30, 31]. Nagashima PPK is caused by biallelic loss of function mutation in *SERPINB7* while, MDM is caused by *SLURP1* gene mutation [20]. Therefore, MDM is genetically distinct from Nagashima PPK [32]. PPKs are diagnosed on the basis of differential diagnosis to find out the

**Table 2** Differential diagnosis of PPKs

Name	Disease Type	Clinical Features	Histopathology	Gene
Mal de Meleda	<b>Diffuse PPK</b>	1. Soon after birth 2. Severe diffuse yellow and waxy thick hyperkeratosis in a 'glove-and-socks' distribution 3. Sharp demarcation 4. Autosomal Recessive	1. Nonepidermolytic pattern 2. Increased stratum lucidum 3. Prominent perivascular inflammatory infiltrate	<i>SLURP1</i>
Unna-Thost		1. Soon after birth to early childhood 2. Diffuse yellowish thick hyperkeratosis with sharp demarcation at the volar border 3. Autosomal Dominant	1. Epidermolytic pattern (perinuclear vacuolization and granular degeneration of keratinocytes in the spinous and granular layer)	<i>KRT1</i> , <i>KRT9</i>
Greither Disease		1. Soon after birth to childhood/adolescence 2. Diffuse red/yellow moderate to severe hyperkeratosis 3. Autosomal Dominant	1. Epidermolytic pattern	<i>KRT1</i>
Nagashima PPK		1. Mostly within infancy 2. Diffuse mild reddish hyperkeratosis, red rim; white spongy appearance after water exposure 3. Autosomal Dominant	1. Nonepidermolytic pattern	<i>SERPINB7</i>
Striate PPK				
Striate Type I PPK	<b>Focal PPK</b>	1. Childhood to adolescence 2. Linear hyperkeratotic distribution on palms and palmar surface of the fingers 3. Focal hyperkeratosis at trauma-prone sites on soles 4. Autosomal Dominant	1. Hyperkeratosis 2. Widening of intercellular spaces in the spinous and granular layer	<i>DSG1</i>
Striate Type II PPK		1. Childhood to early adulthood 2. Linear hyperkeratotic distribution on palms and palmar aspect of fingers 3. Focal hyperkeratosis at trauma-prone sites on soles 4. Autosomal Dominant	1. Hyperkeratosis 2. Widening of intercellular spaces and condensation of the keratin filament network in suprabasal cell layers	<i>DSP</i>
Punctate PPK				
Punctate PPK Type IA	<b>Focal PPK</b>	1. Late childhood to adulthood 2. Multiple hyperkeratotic papules with central indentation 3. Worsening of papules upon exposure to water 4. Autosomal Dominant	1. Hyperkeratosis and hypergranulosis with central epidermal depression	<i>AAGAB</i>
Punctate PPK Type IB		1. Late childhood to adulthood 2. Multiple hyperkeratotic papules with central indentation 3. Autosomal Dominant	1. Hyperkeratosis and hypergranulosis with central epidermal depression	<i>COL14A1</i>
Punctate PPK Type II		1. Puberty to early adulthood 2. Multiple spiny keratosis pits with keratotic plugs (late onset) 3. Autosomal Dominant	1. Columns of parakeratotic corneocytes (cornoid lamellae) 2. Superficial epidermal depression where the granular layer is reduced or absent	Unknown
Punctate PPK Type III		1. Adolescence to adulthood 2. Translucent hyperkeratotic papules, sometimes umbilicated, on lateral aspects of palms and soles 3. Autosomal Dominant	1. Hyperkeratosis and hypergranulosis 2. Decreased number of fragmented elastic fibres	Unknown

PPK, Palmoplantar keratoderma; *SLURP1*, Secreted lymphocyte antigen 6 (LY6)/urokinase-type plasminogen activator receptor (uPAR)-related protein-1; *KRT*, Keratin; *SERPIN7*, serpin peptidase inhibitor, clade B (ovalbumin), member 7; *DSG1*, Desmoglein 1; *DSP*, Desmoplakin; *AAGAB*, Alpha- and gamma-adaptin-binding protein p34; *COL14A1*, Collagen XIV

disease entity. Differential diagnosis of PPK is summarized in Table 2.

## Conclusion

The identification of a novel homozygous nonsense variant in *SLURP1*, and a novel heterozygous nonsense variant in *DSG1*, as likely causes of PPK in the Pakistani families investigated alongside a review of

previously reported variants adds to knowledge of the molecular causes of these conditions. Additionally, the data here provides important information regarding the nature, spectrum and molecular basis of PPK in Pakistan, enabling early clinical intervention, increased awareness regarding inherited disorders present in a community, and aiding diagnosis and counselling.

## Additional file

**Additional file 1: Table S1.** List of candidate pathogenic variants in *SLURP1* gene previously reported in association with Mal de Meleda.  
**Table S2.** List of candidate pathogenic variants in *DSG1* gene previously reported to be associated with Palmoplantar Keratoderma. (DOCX 66 kb)

### Abbreviations

ARS-B: Arylsulfatase B; *DSG1*: Desmoglein 1; HGMD: Human gene mutation data base; MDM: Mal de Meleda; OMIM: Online Mendelian inheritance in man; PPK: Palmoplantar Keratoderma; SAM: Sinobronchial allergic mycosis; *SERPIN7*: Serpin Peptidase Inhibitor, Clade B (Ovalbumin), Member 7; *SLURP1*: Secreted ly6/plaur domain-containing 1 gene; WES: Whole Exome Sequencing

### Acknowledgements

First and foremost, the authors would like to thank the affected individuals and their families for participation in this study. We also thank all of the clinicians and geneticists with whom we have collaborated for their input.

### Authors contributions

Clinical data was collected and collated by AA, while, WA and GVH provided the assistance in genomic DNA extraction. AA, CP1 (Claire Prince), CP2 (Chloe Payne), GVH, AHC, ELB, JF performed genetic testing, analyzed and interpreted the patient data. AA, AG and GVH drafted the manuscript. Study was supervised by ELB, AHC, and AG. All authors reviewed, read and approved the manuscript.

### Authors information

Not applicable

### Funding

This study was partially supported by the Higher Education Commission (HEC) of Pakistan by awarding International Research Support Initiative Program (IRSIP) (Grant No: 1–8/HEC/HRD/2017/7949, PIN: IRSIP 37 BMS 39) to AA and RILD Wellcome Wolfson Centre (Level 4), Royal Devon and Exeter NHS Foundation Trust, UK. Exome/Sanger sequencing and analysis was carried out at RILD Wellcome Wolfson Center UK and was funded by HEC Pakistan and Wellcome Trust UK (to ELB).

### Availability of data and materials

The patient's non-sensitive datasets used and/or analyzed during the current study are available from the corresponding author on reasonable request.

### Ethics approval and consent to participate

The study was approved by the Ethical Review Boards Committee of International Islamic University Islamabad, Pakistan, and the study was carried out in accordance with the principles outlined in the Declaration of Helsinki (1964). Informed written consent was obtained for all participants, including minors (< 16 years of age) with parental consent, for the collection of blood samples with clinical evaluations and family histories performed by a dermatologist.

### Consent for publication

Written informed consents were obtained for publication of clinical and genetic data from individuals > 18 years, while consent for individuals < 18 years of age were given by their parents or legal guardians.

### Competing interests

WA is a member of the editorial board (Associate Editor) of *BMC Medical Genetics*. All other authors declare that they have no competing interests.

### Author details

<sup>1</sup>Department of Biological Sciences, International Islamic University, H-10, Islamabad 44000, Pakistan. <sup>2</sup>College of Medicine and Health, RILD Wellcome Wolfson Centre, University of Exeter, Royal Devon & Exeter NHS Foundation Trust, Barrack Road, Exeter EX2 5DW, UK. <sup>3</sup>Department of Biochemistry, Faculty of Biological Sciences, Quaid-e-Azam University (QAU), Islamabad, Pakistan. <sup>4</sup>Rajarshi Shahi College of Pharmacy, Malvihi Buldana, Maharashtra Post code 443001, India.

Received: 25 April 2019 Accepted: 2 August 2019

Published online: 23 August 2019

### References

- Patel S, Zirwas M, English JC. Acquired palmoplantar keratoderma. *Am J Clin Dermatol*. 2007;8(1):1–1.
- Has C, Technau-Hafsi K. Palmoplantar keratodermas, clinical and genetic aspects. *J Dtsch Dermatol Ges*. 2016;149(2):3–142.
- Guerra L, Castori M, Didona B, Castiglia D, Zambruno G. Hereditary palmoplantar keratodermas. Part I. non-syndromic palmoplantar keratodermas: classification, clinical and genetic features. *J Eur Acad Dermatol Venereol*. 2018;32(5):704–19.
- Sakiyama T, Kubo A. Hereditary palmoplantar keratoderma "clinical and genetic differential diagnosis". *J Dermatol*. 2016;43(3):264–74.
- Fatović-Ferencić S, Holubar K. The portrait and paper of a forgotten hero—Luca Stulli (1772-1828) and the mal de Meleda of yesteryear: a 175-year anniversary. *J Invest Dermatol*. 2001;116(1):198.
- Bergqvist C, Kadara H, Hamie L, Nemer G, Safi R, Karouni M, Marrouche N, Abbas O, Hasbani DJ, Kibbi AG, Nassar D. *SLURP-1* is mutated in mal de Meleda, a potential molecular signature for melanoma and a putative squamous lineage tumor suppressor gene. *Int J Dermatol*. 2018;57(2):162–70.
- Itin PH, Fistorol SK. Palmoplantar keratodermas. *Clin Dermatol*. 2005;23(1):15–22.
- Perez C, Khachemoune A. Mal de Meleda: a focused review. *Am J Clin Dermatol*. 2016;17(1):63–70.
- Fischer J, Bouadjar B, Heilig R, Huber M, Lefèvre C, Jobard F, Macari F, Bakija-Konsuo A, Ait-Belkacem F, Weissenbach J, Lathrop M. Mutations in the gene encoding *SLURP-1* in mal de Meleda. *Hum Mol Genet*. 2001;10(8):875–80.
- Tjiu JW, Lin PJ, Wu WH, Cheng YP, Chiu HC, Thong HY, Chiang BL, Yang WS, Jee SH. *SLURP1* mutation-impaired T-cell activation in a family with mal de Meleda. *Br J Dermatol*. 2011;164(1):47–53.
- Lyukmanova EN, Shulepko MA, Kudryavtsev D, Bychkov ML, Kulbatskii DS, Kasheverov IE, Astapova MV, Feofanov AV, Thomsen MS, Mikkelsen JD, Shenkarev ZO. Human secreted Ly-6/uPAR related protein-1 (*SLURP-1*) is a selective allosteric antagonist of  $\alpha 7$  nicotinic acetylcholine receptor. *PLoS One*. 2016;11(2):0149733.
- Rickman L, Šimrak D, Stevens HP, Hunt DM, King IA, Bryant SP, Eady RA, Leigh IM, Arnemann J, Magee AI, Kelsell DP. N-terminal deletion in a desmosomal cadherin causes the autosomal dominant skin disease striate palmoplantar keratoderma. *Hum Mol Genet*. 1999;8(6):971–6.
- Milingou M, Wood P, Masouye I, McLean WH, Borradori L. Focal palmoplantar keratoderma caused by an autosomal dominant inherited mutation in the desmoglein 1 gene. *Dermatol*. 2006;212(2):117–22.
- Keren H, Bergman R, Mizrahi M, Kashi Y, Sprecher E. Diffuse nonepidermolytic palmoplantar keratoderma caused by a recurrent nonsense mutation in *DSG1*. *Arch Dermatol*. 2005;141(5):625–8.
- Samuelov L, Sarig O, Harmon RM, Rapaport D, Ishida-Yamamoto A, Isakov O, Koetsier JL, Gat A, Goldberg I, Bergman R, Spiegel R. Desmoglein 1 deficiency results in severe dermatitis, multiple allergies and metabolic wasting. *Nat Genet*. 2013;45(10):1244.
- Favre B, Plantard L, Aeschbach L, Brakch N, Christen-Zaech S, de Viragh PA, Sergeant A, Huber M, Hohl D. *SLURP1* is a late marker of epidermal differentiation and is absent in mal de Meleda. *J Invest Dermatol*. 2007; 127(2):301–8.
- Arredondo J, Chernyavsky AI, Webber RJ, Grando SA. Biological effects of *SLURP-1* on human keratinocytes. *J Invest Dermatol*. 2005;125(6):1236–41.
- Grando SA, Pittelkow MR, Schallreuter KU. Adrenergic and cholinergic control in the biology of epidermis: physiological and clinical significance. *J Invest Dermatol*. 2006;126(9):1948–65.
- Musulmanoglu MH, Saracoglu N, Cilingir O, et al. A novel mutation in the ARS (component B) gene encoding *SLURP-1* in a Turkish family with mal de Meleda. *Br J Dermatol*. 2006;155(2):467–9.
- Fischer J, Bouadjar B, Heilig R, Huber M, Lefèvre C, Jobard F, Macari F, Bakija-Konsuo A, Ait-Belkacem F, Weissenbach J, Lathrop M. Mutations in the gene encoding *SLURP-1* in mal de Meleda. *Hum Mol Genet*. 2001;10(8):875–80.
- Taylor JA, Bondavalli D, Monif M, Yap LM, Winship I. Mal de Meleda in Indonesia: mutations in the *SLURP1* gene appear to be ubiquitous. *Australas J Dermatol*. 2014;57(1):11–3.
- Zhang J, Cheng R, Ni C, Liang J, Yao Z. First mal de Meleda report in Chinese mainland: two families with a recurrent homozygous missense mutation in *SLURP-1*. *J Eur Acad Dermatol Venereol*. 2015;30(5):871–3.

23. Shah K, Nasir A, Shahzad S, Khan S, Ahmad W. A novel homozygous mutation disrupting the initiation codon in the *SLURP1* gene underlies mal de Meleda in a consanguineous family. *Clin Exp Dermatol*. 2016;41(6):675–9.
24. Hammers CM, Stanley JR. Desmoglein-1, differentiation, and disease. *J Clin Invest*. 2013;123(4):1419–22.
25. Getsios S, Simpson CL, Kojima SI, Harmon R, Sheu LJ, Dusek RL, Cornwell M, Green KJ. Desmoglein 1-dependent suppression of EGFR signaling promotes epidermal differentiation and morphogenesis. *J Cell Biol*. 2009;185(7):1243–58.
26. Lovgren ML, McAleer MA, Irvine AD, Wilson NJ, Tavadia S, Schwartz ME, Cole C, Sandilands A, Smith FJD, Zamiri M. Mutations in desmoglein1 cause diverse inherited palmoplantar keratoderma phenotypes: implications for genetic screening. *Br J Dermatol*. 2017;176(5):1345–50.
27. Vodo D, O'Toole EA, Malchin N, Lahav A, Adir N, Saring O, Green KJ, FJD, Sprecher E. Striate palmoplantar kerato-derma resulting from a missense mutation in *DSG1*. *Br J Dermatol* 2018;179(3):755–757.
28. Hovorka O. E. Ehlers Mal de Meleda. *Arch Dermatol Res*. 1897;40:251–6.
29. Mitsuhashi Y, Hashimoto I. Keratosis palmoplantaris Nagashima. *Dermatol*. 1989;179:231.
30. Kabashima K, Sakabe JI, Yamada Y, Tokura Y. "Nagashima-type" keratosis as a novel entity in the palmoplantar keratoderma category. *Arch Dermatol* 2008;144(3):375–379.
31. Kubo A, Shiohama A, Sasaki T, Nakabayashi K, Kawasaki H, Atsugi T, Sato S, Shimizu A, Mikami S, Tanizaki H, Uchiyama M. Mutations in *SERPINB7*, encoding a member of the serine protease inhibitor superfamily, cause Nagashima-type palmoplantar keratosis. *Am J Hum Genet*. 2013;93(5):945–56.
32. Dua-Awereh MB, Shimomura Y, Kraemer L, Wajid M, Christiano AM. Mutations in the desmoglein 1 gene in five Pakistani families with striate palmoplantar keratoderma. *J Dermatol Sci*. 2009;53(3):192–7.

## Publisher's Note

Springer Nature remains neutral with regard to jurisdictional claims in published maps and institutional affiliations.

**Ready to submit your research? Choose BMC and benefit from:**

- fast, convenient online submission
- thorough peer review by experienced researchers in your field
- rapid publication on acceptance
- support for research data, including large and complex data types
- gold Open Access which fosters wider collaboration and increased citations
- maximum visibility for your research: over 100M website views per year

**At BMC, research is always in progress.**

Learn more [biomedcentral.com/submissions](https://biomedcentral.com/submissions)





## Glucosamine HCl-based solid dispersions to enhance the biopharmaceutical properties of acyclovir.

Darshan R. Telange<sup>a</sup>, Snehal B. Bhagat<sup>a</sup>, Arun T. Patil<sup>a</sup>, Milind J. Umekar<sup>a</sup>, Anil M. Pethe<sup>b</sup>, Nishikant A. Raut<sup>c</sup>, Vivek S. Dave<sup>4\*</sup>

<sup>a</sup>Rajarshri Shahu College of Pharmacy, Malvihir, Buldhana, Maharashtra, India

<sup>b</sup>Shobhaben Pratapbhai Patel School of Pharmacy & Technology Management, SVKM'S NMIMS, V. L. Mehta Road, Vile Parle (West) Mumbai, Maharashtra, India

<sup>c</sup>University Department of Pharmaceutical Sciences, R. T. M. Nagpur University, Maharashtra, Nagpur

<sup>d</sup>St. John Fisher College, Wegmans School of Pharmacy, Rochester, NY, USA

Received: June 5, 2019; Accepted: August 6, 2019

Original Article

### ABSTRACT

The objective of the work presented here was to assess the feasibility of using glucosamine HCl as a solid-dispersion (SD) carrier to enhance the biopharmaceutical properties of a BCS class III/IV drug, acyclovir (ACV). The solid-dispersions of acyclovir and glucosamine HCl were prepared by an ethanol-based solvent evaporation method. The prepared formulations characterized by photomicroscopy, scanning electron microscopy (SEM), differential scanning calorimetry (DSC), Fourier transforms infrared spectrophotometry (FTIR), powder x-ray diffractometry (PXRD) and drug content analysis. The functional characterization of ACV-SD was performed by aqueous solubility evaluation, dissolution studies, fasted *versus* fed state dissolution comparison, ex vivo permeability, and stability studies. Photomicroscopy and SEM analysis showed different surface morphologies for pure ACV, glucosamine HCl and ACV-SD. The physical-chemical characterization studies supported the formation of ACV-SD. A 12-fold enhancement in the aqueous solubility of ACV was observed in the prepared solid dispersions, compared to pure ACV. Results from *in vitro* dissolution demonstrated a significant increase in the rate and extent of ACV dissolution from the prepared ACV-SD formulations, compared to pure ACV. The rate and extent of ACV permeability across everted rat intestinal membrane were also found to be significantly increased in the ACV-SD formulations. Under fed conditions, the rate and extent of the *in vitro* dissolution of ACV from the formulation was appreciably greater compared to fasted conditions. Overall, the results from the study suggest the feasibility of utilizing glucosamine HCl as a solid dispersion carrier/excipient for enhancement of biopharmaceutical properties of acyclovir, and similar drugs with low solubility/permeability characteristics.

**KEY WORDS:** Acyclovir, ACL, glucosamine HCl, solid dispersion, solubility, permeability, excipients

### INTRODUCTION

Modern drug discovery techniques, which include high throughput screening and combinatorial chemistry, have generated new molecules with solubility characteristics that result in lower and inconsistent oral bioavailability (1). Over half of all newly discovered drugs appears

to fall into biopharmaceutics classification system's (BCS) class II (↓ solubility, ↑ permeability), Class III (↑ solubility, ↓ permeability) or class IV (↓ solubility, ↓ permeability) (2). These drugs exhibit dissolution and/or permeation rate-limited absorption. For these drugs, enhancement of dissolution rate and/or permeability is vital to attain suitable blood concentration to achieve optimal bioavailability for therapeutic effect (3-5). Thus, for a formulation development team, there is a consistent and well-justified need to explore

\*Corresponding address: Vivek S. Dave, St. John Fisher College, Wegmans School of Pharmacy, Rochester, NY, 14534, Tel: 1-585-385-5297, Fax: 1-585-385-5295, E-mail: [vdave@sjfc.edu](mailto:vdave@sjfc.edu)

approaches that improve the dissolution and/or permeability characteristics of such drugs.

Among the popular approaches explored in the past decade to achieve this goal include the micronization of drugs, formulation of drugs into liposomes, microspheres, microemulsions, inclusion complexes, nanoparticles, self-micro emulsifying drug delivery systems, solid dispersions, and other non-traditional drug delivery systems (6-14). Among these, formulating drugs into solid dispersions to improve their biopharmaceutical properties has gained widespread traction and acceptance. Solid dispersions are typically formed by uniformly dispersing one, or more, APIs into a hydrophilic matrix carrier using thermal, mechanical, co-solubilizing or a combination of one or more similar techniques (15, 16). Within a solid dispersion, the solubility and permeability of the API is reported to be improved by, a) the reduction of particle size of the drug to sub-micron or smaller, allowing increased surface area for dissolution, b) the alteration of a crystalline drug to a high energy amorphous state, and c) increasing wettability of the drug particles in an aqueous environment (16, 17). The development of a successful solid dispersion often depends on the choice of the carrier material, as well as, the processing method.

Acyclovir is an antiviral drug, commonly prescribed for the treatment of infections caused by the herpes simplex viruses (HSV-1 and HSV-2) and the varicella-zoster virus. Depending on the available strength of the tablets, acyclovir has been classified as either a BCS class III or a class IV drug (18). Upon oral administration, acyclovir exhibits low oral bioavailability (~15-30%) (19). The low bioavailability of acyclovir is attributed to its poor aqueous solubility, as well as, low permeability (20-23). Therefore, acyclovir was selected as a model drug for this study with the objective to improve its dissolution and permeability characteristics.

Glucosamine is a naturally occurring amino-monosaccharide obtained from glucosamine-6-phosphate *via* a hexosamine biosynthetic pathway. Structurally, it is a 2-amino-2-deoxy- $\beta$ -D-glucopyranose with the molecular formula ( $C_6H_{13}NO_5$ ).

It is a non-toxic and a highly water-soluble (320 mg/mL) compound (24, 25). Among its salts, that is hydrochloride (HCl), sulfate and N-acetyl, the HCl salt is pharmaceutically acceptable due to its high aqueous solubility and physical stability. The hydrophilic nature of glucosamine HCl is reported to improve drugs with poor aqueous solubility and permeability by improving particle wettability in an aqueous environment (26). Despite its potential drug delivery optimizing benefits, the usage and applications of glucosamine HCl as a carrier in the designing of novel drug delivery systems remains largely unexplored. In recent years, only a few publications originating from the group of Al-Hamidi *et. al.* have reported the potential for using glucosamine HCl as a solid dispersion carrier (26, 27). While useful and informative, these studies can be considered insufficient in terms of material characterization and functional analysis of the formulations.

Therefore this study describes a systematic and comprehensive feasibility analysis of using glucosamine HCl as a solid dispersion carrier for improving the dissolution and/or permeability characteristics of acyclovir. For the study, acyclovir solid dispersion formulations (ACV-SD) with increasing ratios of glucosamine HCl were prepared using an ethanol-based, solvent-evaporation method. The prepared ACV-SD were subjected to physical-chemical characterization with scanning electron microscopy, particle size and zeta potential analysis, thermal analysis, Fourier transforms infrared spectroscopy, powder x-ray diffractometry, aqueous solubility, and drug content analysis. The ACV-SD were further characterized for their functionality via dissolution and permeability studies, and fasted- and fed- state dissolution studies. Finally, the influence of controlled-storage conditions on the functional attributes of ACV-SD was evaluated by conducting a preliminary stability study for a period of six months.

## MATERIALS AND METHODS

### Materials

Acyclovir was obtained from Zim Laboratories Ltd., Nagpur, India. D (+) Glucosamine hydrochloride was



sourced from Sigma-Aldrich Corporation, St. Louis, MO, USA. Dichloromethane, ethanol, glacial acetic acid, soy lecithin, methanol, n-octanol, sodium hydroxide, and sodium taurocholate were acquired from Loba Chemical Pvt. Ltd., Mumbai, India. Calcium chloride, glucose, magnesium sulfate, potassium chloride, potassium dihydrogen phosphate, sodium chloride, and sodium bicarbonate were sourced from Merck Ltd. Mumbai, India. All other chemicals/solvents used were of analytical grade and used as received.

### Preparation of acyclovir solid dispersion (ACV-SD)

Solid dispersions of acyclovir (ACV-SD) using glucosamine HCl as a carrier were prepared using different drug:carrier ratios (1:1, 1:2, 1:3, 1:4, and 1:5) according to the method previously described by Dhore *et al.* (28). Briefly, acyclovir was weighed and dissolved in 10 mL ethanol. The ethanolic solution of acyclovir was then added to previously weighed glucosamine HCl in a mortar and blended thoroughly. The blending/trituration was continued until the ethanol was completely evaporated, forming a uniform dispersion. Complete evaporation of any residual ethanol was ensured by vacuum drying the samples at 40°C for 12 hours. The dried ACV-SD sample powders were stored in amber glass vials (flushed with nitrogen) at controlled room temperature (25°C) until needed. The composition of the prepared ACV-SD is shown in Table 1.

**Table 1** Composition of the prepared acyclovir-glucosamine hydrochloride solid-dispersion formulations

FORMULATION	DRUG (MG)	CARRIER (MG)
ACV-SD1	100	100
ACV-SD2	100	150
ACV-SD3	100	200
ACV-SD4	100	250
ACV-SD5	100	300

### Physical-chemical characterization of ACV-SD

#### Photomicroscopy and scanning electron microscopy (SEM)

The preliminary microscopic assessment of pure

ACV, glucosamine HCl and the prepared ACV-SD was carried out using a digital microscope (Model: DM2500, Leica Microsystems, Germany). The samples for analysis were prepared by dispersing ~10 mg of either the drug, the carrier or the prepared formulation in 5 mL distilled water. A droplet from the uniformly mixed dispersion was then placed on a clean glass slide and observed under the microscope. The images of the samples were captured at different resolutions.

Additionally, individual samples were also examined for their surface characteristics using a scanning electron microscope (Model: Supra<sup>®</sup> 55, Carl Zeiss NTS Ltd., Germany). Briefly, the sample (~50g) was spread as a thin layer on a double-faced carbon tape, placed on the aluminum platform, which was then placed in the sample holder of the microscope. The sample was then coated with a thin layer of gold (~400 Å) using a sputter coater (Model: Supra<sup>®</sup> 55). The samples were scanned at an accelerating voltage of 10 kV, and the equipment-accompanied software (SmartSEM<sup>®</sup>, TV mode) was used to develop and record the images at different magnifications.

#### Particle size and zeta potential analysis

The particle size distribution of the prepared ACV-SD was performed on a Photon Cross Correlation Spectrometer (Model: NANOPHOX Sympatec, GmbH, Clausthal-Zellerfeld, Germany) with dynamic light scattering using a procedure reported by our laboratory earlier (29). The test samples were prepared by dispersing ACV-SD in deionized water. The analysis was performed at an operating sensitivity of 1 nm to 10 µm, and the particle count rate was optimized by the associated software.

The prepared ACV-SD were also analyzed for zeta potential using a Nano Particle Analyzer (Model: NanoPlus<sup>TM</sup>-2, Particulate system, Norcross, GA, USA). The analysis was carried out at a controlled temperature (25°C) and an operating range of -200 to +200 mV.

#### Thermal analysis

To evaluate any interactions between ACV and

glucosamine HCl, a differential scanning calorimeter (Model: Q20, TA Instrument, Inc., New Castle, DE, USA) was used to record the thermal behaviors of pure ACV, pure glucosamine HCl, the physical mixture (PM, 1:3) of pure ACV and glucosamine HCl, and the prepared ACV-SD. Thermograms of these samples were compared and analyzed. Individual samples (~ 2 mg) were press-sealed in aluminum pans and analyzed on the equipment previously calibrated with an indium standard. Each sample was subjected to a heating cycle from 0°C to 400°C at a ramp rate of 10°C/min, under a continuous purge of nitrogen (50 mL/min). The universal analysis software (Version 4.5A, build 4.5.0.5, TA Instruments, Inc., New Castle, DE, USA) accompanied by the instrument was used to analyze and interpret the obtained thermograms.

#### Fourier transforms infrared spectroscopy (FTIR)

Pure ACV, glucosamine HCl, PM, and ACV-SD samples were subjected to FTIR analysis in an attempt to understand their chemical differences as well as any interactions between the ACV and glucosamine HCl, either in a physical mixture or within the prepared dispersion. The spectra were collected using an FTIR spectrophotometer (Model: FTIR-8300, Shimadzu, Kyoto, Japan) following the procedure reported by Telange *et al.* (30), and compared in order to identify the occurrence of any intermolecular interactions.

#### Powder x-ray diffractometry (PXRD)

The crystal characteristics of the drug, the carrier, their physical mixture (1:3), and the prepared solid dispersion were investigated by PXRD. The diffractograms were obtained on a bench-top x-ray diffractometer (MODEL: D8 ADVANCE, Bruker AXS, Inc., Madison, WI, USA), using the method reported previously by Telange *et al.* (29).

#### Estimation of ACV content in ACV-SD

The ACV content in the prepared ACV-SD was estimated spectrophotometrically, following a procedure described by Chaudhary *et al.* (31). The appropriate quantity of ACV-SD powder (containing

~100 mg ACV) was dissolved in 100 mL phosphate buffer (0.05 M, pH 6.8). The resulting solution was filtered (membrane filter, 0.45 µm), and after relevant sequential dilutions, analyzed using a UV-visible spectrophotometer (MODEL: V-630, JASCO International Co., Ltd., Tokyo, Japan) at 251 nm. The sample absorbance values were compared against those from a blank (a solution of glucosamine HCl in phosphate buffer) to calculate the amount of free ACV in the ACV-SD. The ACV content (%) incorporated in the prepared SD formulations was calculated using Equation 1.

$$\text{ACV content (\%)} = \frac{\text{total ACV (mg)} - \text{free drug (mg)}}{\text{total ACV (mg)}} \times 100 \quad \text{Eq. 1}$$

#### Aqueous solubility analysis

The aqueous solubilities of pure ACV, ACV in the physical mixture, and ACV in the prepared dispersions were determined using a procedure mimicking the one described by Al-Hamidi *et al.* (27). Excess amounts of samples were individually dispersed in 10 mL distilled water in screw-cap glass vials and agitated on a rotary shaker (Model: RS-24 BL, REMI Laboratory Instruments, Remi House, Mumbai, India) at 37°C for 24 hours. The dispersions were then filtered (0.45 µm), diluted, and the absorbance of the resulting solutions was measured on a UV-visible spectrophotometer (MODEL: V-630, JASCO International Co., Ltd., Tokyo, Japan) at 251 nm. The absorbance values, after comparison with a blank and a standard solution of ACV, were used to calculate the aqueous solubility of ACV.

#### Functional characterization of ACV-SD

##### *In vitro* dissolution studies

Comparative assessment of the release pattern of pure ACV and ACV from ACV-SD was performed using a USP Type II (paddle) dissolution equipment (Model: TDT-08LX, Electrolab India Pvt. Ltd., Mumbai, India). Each dissolution run was conducted by dispersing pure ACV (40 mg) or ACV-SD (~40 mg ACV) in the dissolution vessel containing freshly

prepared phosphate buffer (900 mL, 0.05 N, pH 6.8) maintained at 37°C. The experiment was carried out for 120 minutes at 100 RPM stirring speed. Sample aliquots for testing were collected at 10 minute intervals and replaced with equal volumes of fresh medium. The test samples, after filtration and appropriate dilutions, were measured for absorbance using a UV-visible spectrophotometer (MODEL: V-630, JASCO International Co., Ltd., Tokyo, Japan) at 251 nm. The absorbance values, after comparison with a blank and a standard solution of ACV, were used to calculate the cumulative dissolution profiles of ACV and ACV-SD.

### **Influence of fasted versus fed-state media**

The influence of fasted *versus* fed state on the dissolution behavior of pure ACV and ACV-SD was assessed by conducting dissolution tests using standard Fasted (FaSSIF) and Fed-state (FeSSIF) dissolution media. The media were prepared using the procedure reported by Klein *et al.* (32). The dissolution was performed on a USP Type II (paddle) dissolution test apparatus (Model: TDT-08LX, Electrolab India Pvt. Ltd., Mumbai, India). Each dissolution run was conducted by dispersing pure ACV (100 mg) or ACV-SD (~100 mg ACV) in the dissolution vessel containing either FaSSIF (500 mL) or FeSSIF (1000 mL) maintained at 37°C. The dissolution was carried out for 120 min at a paddle stirring speed of 50 RPM. Aliquots of samples were collected at 10 minute intervals for testing and replaced with an equal volume of the blank medium. The test samples, after filtration and appropriate dilutions, were measured for absorbance on a UV-visible spectrophotometer (Model: V-630, JASCO International Co., Ltd., Tokyo, Japan) at 248.2 nm (FaSSIF) or 272 nm (FeSSIF). The absorbance values were used to calculate the cumulative dissolution profiles of ACV and ACV-SD in respective media.

### **Permeability across a biological membrane**

The biological permeability of pure ACV and ACV in the prepared dispersion was assessed using the everted

rat intestine method previously reported by Dixit *et al.* (33). The details of the method, including the design and assembly of the apparatus, the use of experimental animals, and so on has been reported previously and followed as described therein (34). Briefly, the isolated intestinal membrane was mounted on the apparatus filled with Krebs solution (250 mL) as a permeation medium. The test sample solutions i.e., pure ACV (100 µg/mL) or ACV-SD (~100 µg/mL), prepared using Krebs solution, were placed in the apparatus on the mucosal side of the membrane. The medium was maintained at 37°C and continuously stirred at 25 RPM for a period of 120 minutes. Aliquots of samples were withdrawn at regular intervals from the serosal side of the membrane, and after filtration and appropriate dilutions, were measured for absorbance using a UV-visible spectrophotometer (MODEL: V-630, JASCO International Co., Ltd., Tokyo, Japan) at 250.4 nm. The obtained absorbance values were used to calculate the cumulative permeability profiles of ACV and ACV-SD.

### **Preliminary stability assessment**

The optimized ACV-SD formulation i.e., ACV-SD3 was evaluated for its functional stability upon storage under controlled storage conditions (25°C at 60% RH). The samples were packaged in screw-capped, high-density polyethylene (HDPE), amber-colored bottles, and stored in an environmental chamber (Model: TS00002009, Mumbai, Maharashtra, India) for a period of six months. At the end of six months, the samples were retrieved and subjected to dissolution and permeability studies using the respective procedures described above.

### **Statistical analysis**

The results are presented as mean  $\pm$  standard deviation. The statistical analysis for comparing differences between test samples was performed using a one-way analysis of variance (ANOVA) followed by a Dunnett's or a Student's t-test. P values of  $\leq 0.05$  were considered as a statistically significant difference.



## RESULTS AND DISCUSSION

## Physical-chemical characterization of ACV-SD

**Photomicroscopy and scanning electron microscopy (SEM)**

Microscopic images of pure ACV, pure glucosamine HCl, and ACV-SD, captured at 20X magnification are shown in Figure 1 (A, B, and C). Pure ACV (Figure 1A) appeared as small, regular crystals with well-defined geometric faces and edges. The morphology of these crystals appeared to correspond to the monoclinic polymorphic form V of ACV (35). The glucosamine HCl particles (Figure 1B) appeared to be relatively larger, globular particles with a smooth surface. The particles of ACV-SD (Figure 1C) appeared as non-uniform, clusters with ill-defined morphology. The defining characteristics of pure ACV or pure glucosamine HCl were absent in ACV-SD.

Further analysis of these particles using SEM imaging confirmed the observations from the photomicroscopic images (Figure 1a, 1b, and 1c). Pure ACV exhibited a crystalline, regular structure with geometric angles (Figure 1a). Pure glucosamine HCl showed larger particles with a rounded, smooth surface. The ACV-SD particles appeared as irregular clusters/aggregates formed as a result of the physical interaction between ACV and glucosamine HCl.

**Particle size and zeta potential analysis**

The mean particle size and zeta potential are considered relevant markers indicative of the physical stability of sub-micron particles dispersed in a liquid medium (29). Particles sizes  $\leq 500$  nm are known to prefer endocytosis as a major pathway of transport across biological membranes (36). The mean particle size of the prepared ACV-SD was  $\sim 120$  nm with a polydispersity index (PDI) of 31.06 (Figure 2A). The

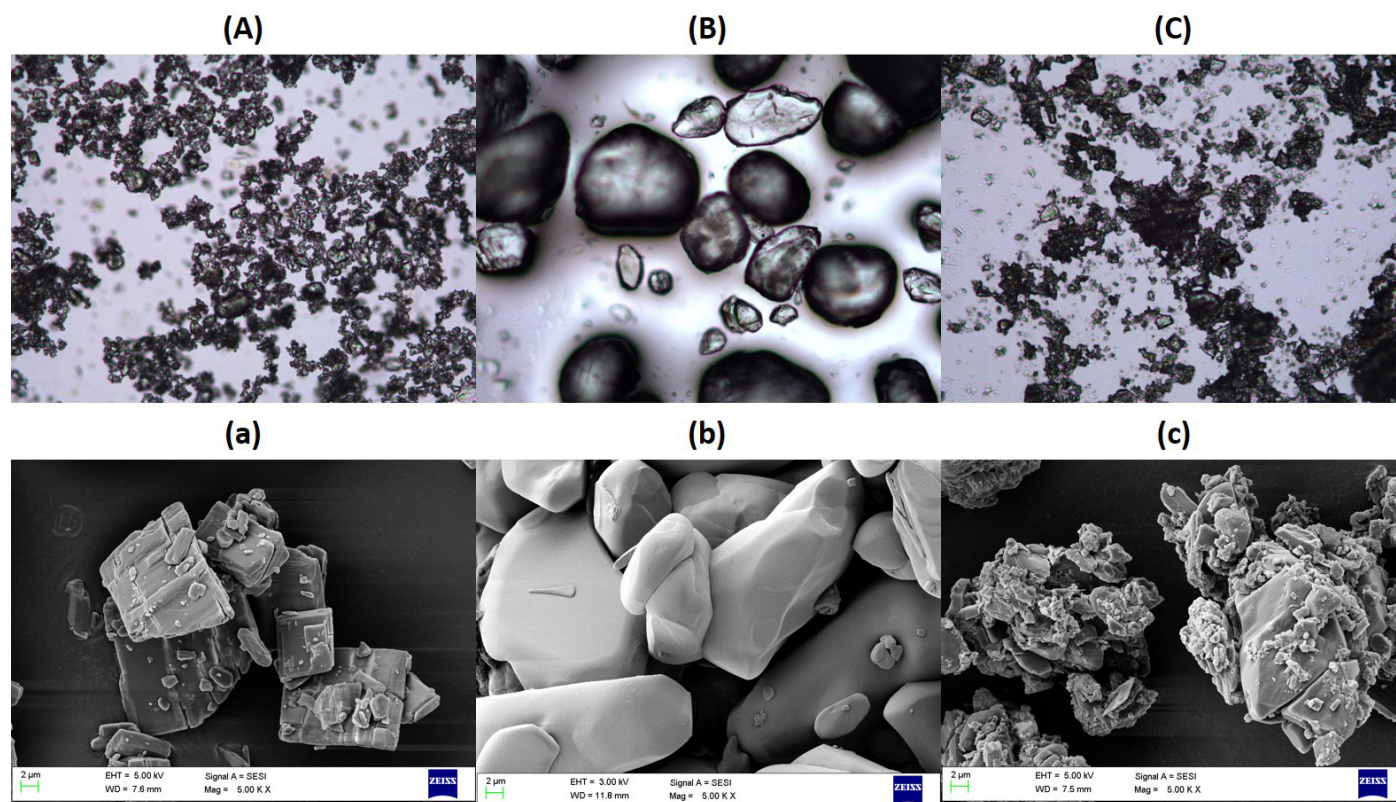


**Figure 1** Photomicroscopy images of (A) pure acyclovir, (B) pure glucosamine HCl, and (C) acyclovir-glucosamine HCl solid dispersion. Scanning electron microscopy images of (a) pure acyclovir, (b) pure glucosamine HCl, and (c) acyclovir-glucosamine HCl solid dispersion (ACV-SD).

prepared formulation thus has a sub-micron particle size and a narrow distribution.

Zeta potential ( $\zeta$ ) often indicates the relative physical stability of multiparticulate, disperse systems. The measured zeta potential value of the prepared ACV-SD formulation was  $-39.43 \pm 0.23$  mV (Figure 2B), indicating that the prepared formulation dispersion is relatively stable, and bereft of any aggregation

potential (28).

### Thermal analysis

Physical interactions, if any, between the components of a formulation, are generally quite conveniently assessed using comparative thermal analysis. Such interactions are generally revealed in the form of appearance, disappearance, shifting, or changes

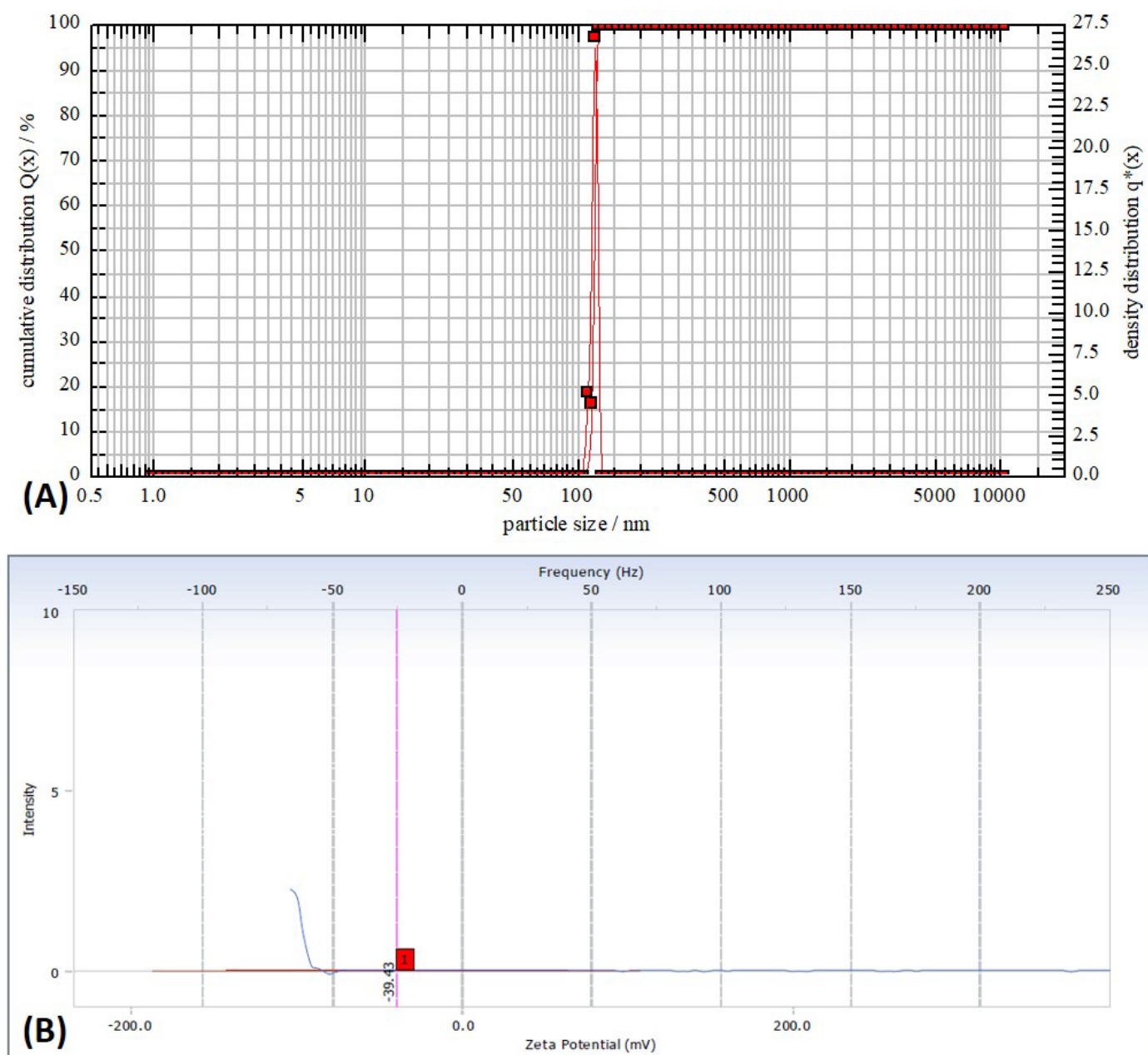


**Figure 2** Particle size distribution (A) and zeta potential (B) of the prepared ACV-SD formulation.

in the onset and/or relative areas of the peaks as a function of controlled temperature increases. These interactions may indicate melting, degradation, and/or incompatibilities between the components of the formulation.

Figure 3 (A, B, C, and D) shows the thermograms obtained from the DSC analysis of pure ACV, pure glucosamine HCl, the physical mixture (PM, 1:3) of pure ACV and glucosamine HCl, and the prepared ACV-SD. The thermogram of pure ACV (Figure 3A) exhibited a sharp peak at  $\sim 256^{\circ}\text{C}$ , indicative of

the melting temperature of ACV. Another minor endothermic event was observed for pure ACV between  $\sim 60^{\circ}\text{C}$  and  $\sim 175^{\circ}\text{C}$  (not apparent in the figure). This event may be attributed to the phase transition of polymorphic hydrate form V to anhydrous form III in the range of  $65^{\circ}\text{C}$  and  $100^{\circ}\text{C}$ , and thereafter from form III to anhydrous form VI at higher temperatures. These changes in the thermal characteristics of ACV are not uncommon and have been reported earlier (9, 10, 37). The thermogram of glucosamine HCl (Figure 3B) revealed two, broad, fused endothermic peaks; a larger peak with an onset at  $\sim 190^{\circ}\text{C}$  and a smaller peak

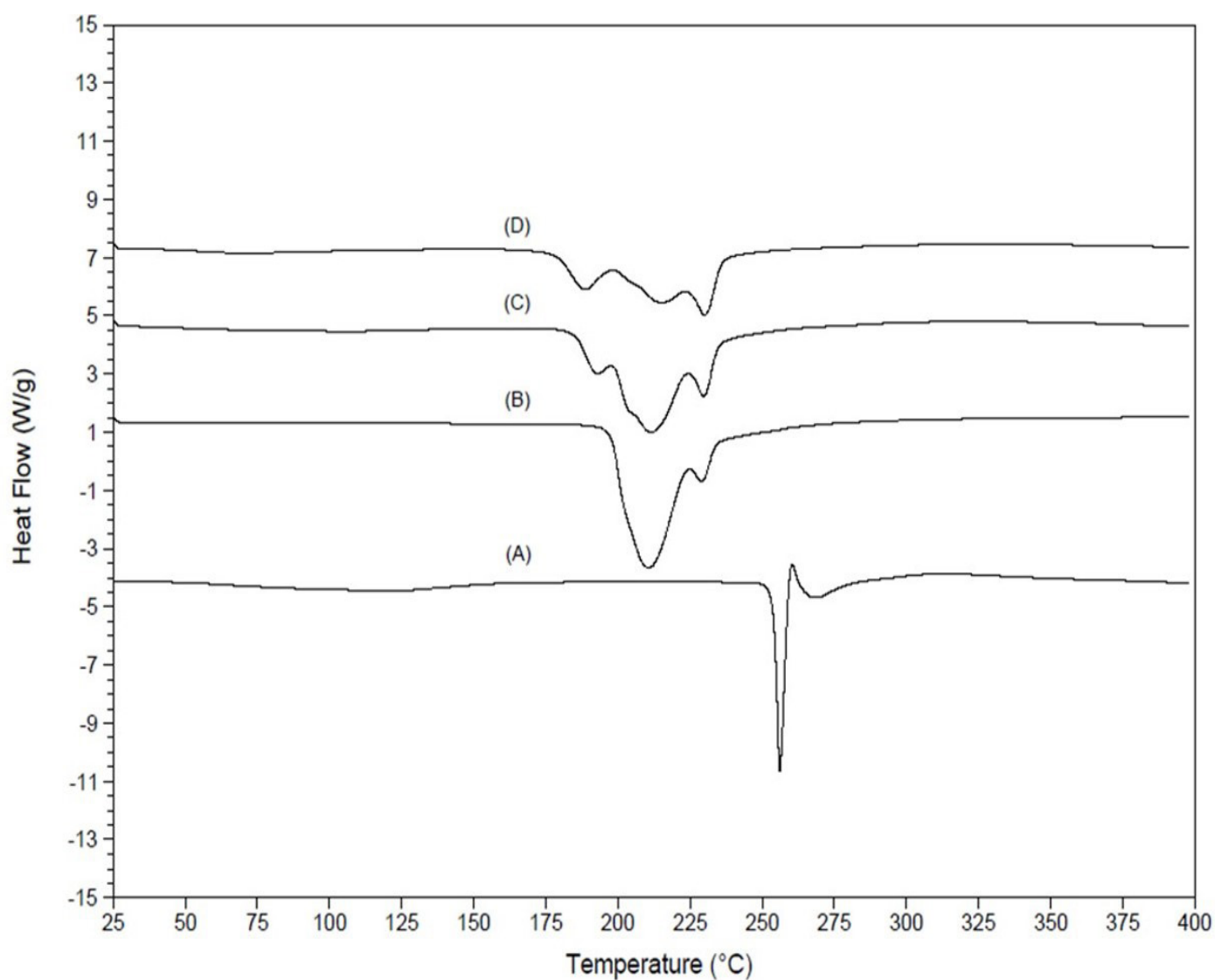


**Figure 3** DSC thermograms of (A) pure ACV, (B) pure glucosamine HCl, (C) the physical mixture (1:3) of ACV and glucosamine HCl, and (D) the prepared ACV-SD formulation.



at  $\sim 229^\circ\text{C}$ . The first peak is likely associated with the melting of glucosamine HCl, and the second, smaller peak may be associated with its degradation. These results are in agreement with previously published reports (26, 27). The thermograms of the physical mixture (Figure 3C) exhibited broad, fused peaks similar to that of pure glucosamine HCl, along with the disappearance of the melting peak of ACV. It is likely that with increasing temperatures, glucosamine HCl melted earlier at around  $190^\circ\text{C}$  and ACV dispersed/dissolved in the carrier matrix in situ. The thermogram of ACV-SD (Figure 3D) revealed broad, diffused endothermic peaks that were uncharacteristic of either pure ACV or pure glucosamine HCl. The absence of defining peaks of ACV and glucosamine HCl in ACV-SD thermogram is expected to owe the possibility that ACV is molecularly dispersed into the carrier matrix, resulting in partial amorphization of ACV.

#### Fourier transform infrared spectroscopy (FTIR)

The spectra obtained from the infrared analysis of pure ACV, pure glucosamine HCl, the physical mixture (PM, 1:3) of pure ACV and glucosamine HCl, and the prepared ACV-SD are shown in Figure 4A, 4B, 4C, and 4D, respectively. For pure ACV (Figure 4A), characteristic absorption bands were located at  $\sim 3622\text{ cm}^{-1}$  (primary amine) and  $3411\text{ cm}^{-1}$  (secondary amine, N-H stretching). Additional peaks typically associated with ACV were found at  $\sim 1712\text{ cm}^{-1}$  (C=O stretching),  $\sim 1630\text{ cm}^{-1}$  and  $\sim 1609\text{ cm}^{-1}$  (amine),  $\sim 1483\text{ cm}^{-1}$  (O-H stretching), and  $\sim 1347\text{ cm}^{-1}$  (C-H stretching). These observations were consistent with previous findings (10, 38). The FTIR spectrum of glucosamine HCl (Figure 4B) exhibited a characteristic absorption peak at  $\sim 3291\text{ cm}^{-1}$  (N-H and O-H stretching). Other peaks related to glucosamine were observed at  $\sim 3000\text{ cm}^{-1}$  and  $2881\text{ cm}^{-1}$  (-C-H stretching),  $\sim 1618\text{ cm}^{-1}$  and  $1537\text{ cm}^{-1}$  (N-H bending),  $\sim 1140\text{ cm}^{-1}$  (asymmetric

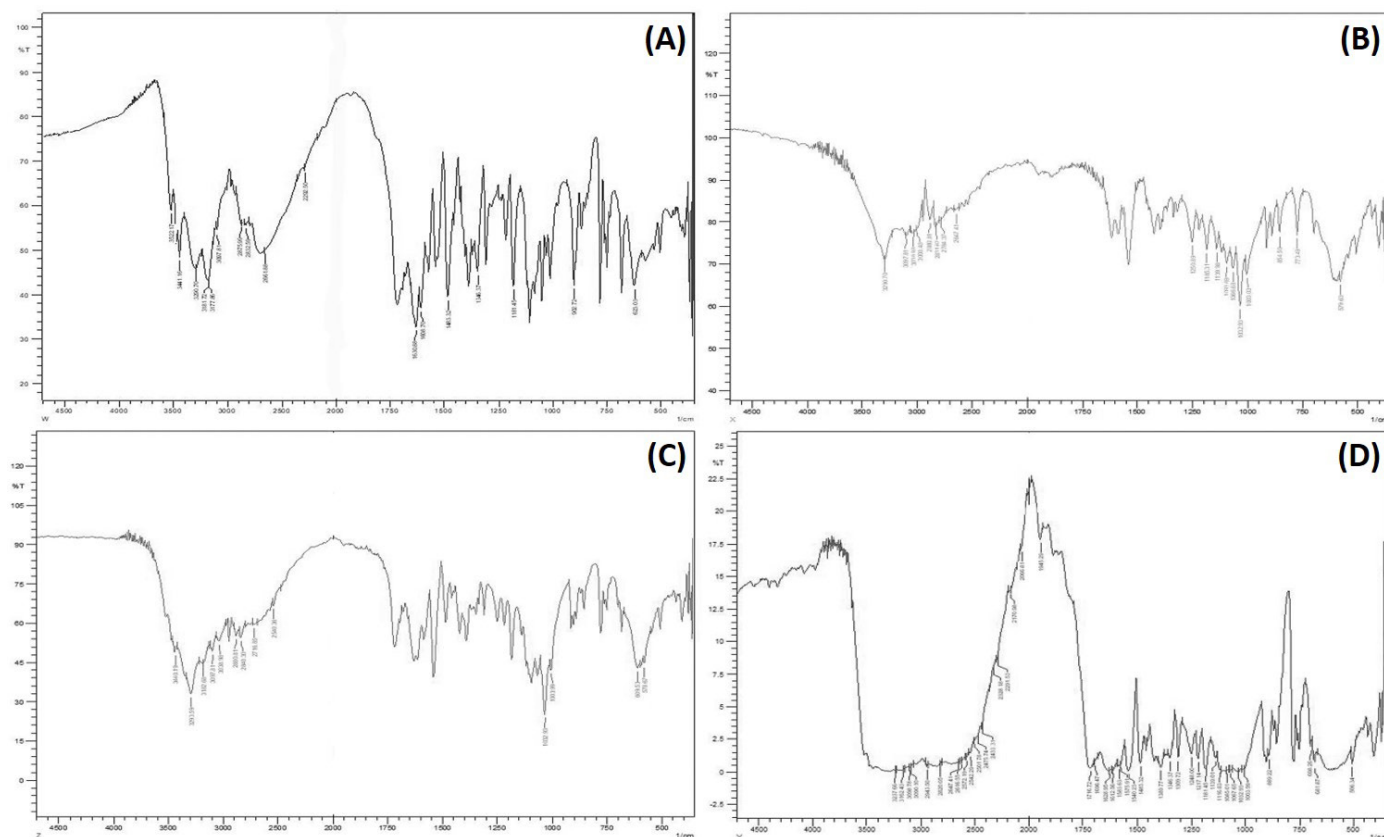


**Figure 4** FTIR spectra of (A) pure ACV, (B) pure glucosamine HCl, (C) the physical mixture (1:3) of ACV and glucosamine HCl, and (D) the prepared ACV-SD formulation.

C-O-C stretching) and  $\sim 1094\text{ cm}^{-1}$  (C-O functional group). These results were analogous to those reported earlier (39). The spectrum of the physical mixture of the drug and the carrier (Figure 4C) showed peaks corresponding mostly to glucosamine HCl, albeit with higher absorbance intensities. The higher ratio of glucosamine HCl in the mixture can be attributed to the observed predominance of glucosamine related peaks. The FTIR plot of ACV-SD formulation (Figure 4D) was found to be significantly different compared to those of the individual components. The characteristic peaks associated with pure ACV and pure glucosamine HCl were absent in this spectrum. Several absorption peaks were observed in the region between  $3300\text{ cm}^{-1}$  and  $1085\text{ cm}^{-1}$ . The presence of unique peaks in this spectrum can be likely attributed to hydrogen bonding between the N-H functional group of ACV and the O-H group of glucosamine HCl, and the formation of solid dispersion (10, 27). The formation of solid

dispersion not only helps in solubilizing the API into the hydrophilic carrier but also likely prevents the recrystallization of the drug in the glass solution (40).

### Powder x-ray diffractometry (PXRD)

Powder x-ray diffractometry (PXRD) provides useful information on the crystalline properties and any polymorphic changes in the components of a formulation. The diffractograms obtained from the PXRD analysis of pure ACV, pure glucosamine HCl, the physical mixture (PM, 1:3) of pure ACV and glucosamine HCl, and the prepared ACV-SD are shown in Figure 5 (A, B, C and D). The diffractogram of pure ACV (Figure 5A) showed a sharp, high-intensity peak at  $\sim 7^\circ 2\theta$ , related to ACV crystal structure. Other low-intensity peaks were observed at  $\sim 10.5^\circ$ ,  $21^\circ$ ,  $26^\circ$ , and  $29^\circ$  on the  $2\theta$  scale. All these peaks are associated with the polymorphic form V of ACV and in agreement with earlier published reports (10). The diffraction pattern

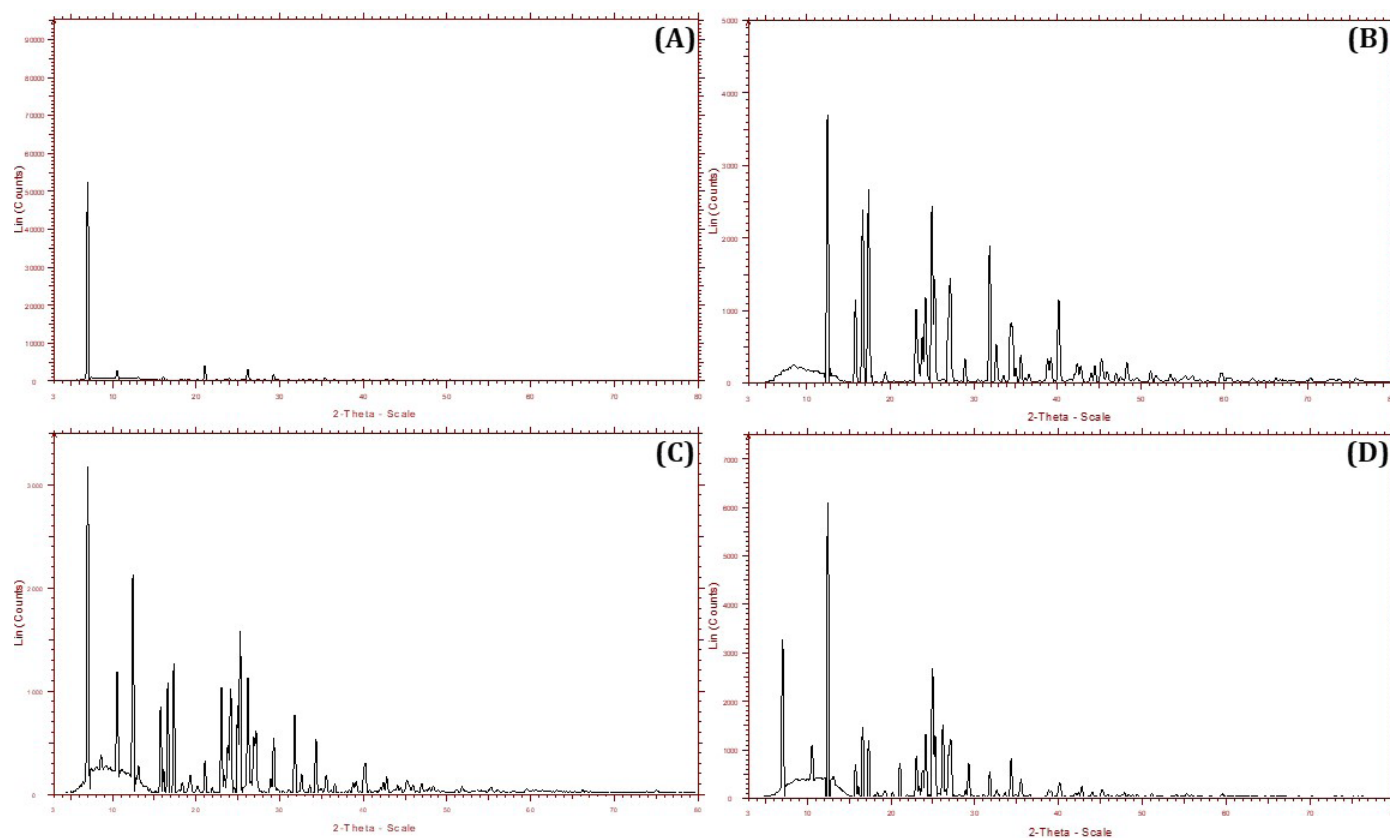


**Figure 5** The x-ray diffractograms of (A) pure ACV, (B) pure glucosamine HCl, (C) the physical mixture (1:3) of ACV and glucosamine HCl, and (D) the prepared ACV-SD formulation.

of glucosamine HCl (Figure 5B) exhibited several low and high-intensity peaks in the region between  $12^\circ 2\theta$  and  $60^\circ 2\theta$ , along with a partial amorphous 'halo' pattern between  $5^\circ 2\theta$  and  $15^\circ 2\theta$ , indicating a mostly crystalline nature of the carrier. The diffractogram was similar to that reported previously in the literature (26). The diffractogram of the physical mixture (Figure 5C) showed a series of peaks between  $7^\circ 2\theta$  and  $43^\circ 2\theta$ . These peaks appeared to those observed with pure ACV and pure glucosamine HCl, albeit with lower intensities for peaks associated with ACV. Finally, the diffractogram of ACV-SD revealed peaks that were of significantly lower in number and intensities compared to the pure components (Figure 5D). The diffractogram appeared to retain the characteristic peaks of the carrier, whereas, ACV-related peaks were greatly minimized. It is likely that ACV is partially amorphized in the prepared solid dispersion.

### Estimation of the ACV content in ACV-SD

The ACV content in the prepared ACV-SD is represented as % ACV incorporated in Table 2. For all ACV-SD formulations, the ACV content was found to be  $> 95\%$  w/w. The formulation ACV-SD3 (drug-carrier ratio of 1:3) showed the highest incorporation efficiency ( $98.17 \pm 0.49\%$ ) and was used as an optimal formulation for most of the characterization studies. The high incorporation efficiency of ACV in the prepared formulation supported the selection of carrier and the robustness of the formulation approach.

### Aqueous solubility analysis

The results obtained from the aqueous solubility

**Table 2** Drug content of acyclovir in prepared solid-dispersion formulations

FORMULATION	DRUG CONTENT (% w/w)*
ACV-SD1	$95.30 \pm 0.65$
ACV-SD2	$97.21 \pm 1.32$
ACV-SD3	$98.17 \pm 0.49$
ACV-SD4	$96.10 \pm 1.01$
ACV-SD5	$96.44 \pm 1.20$

\*All results are expressed as mean  $\pm$  Std. Dev., n=3

analysis of pure ACV, the physical mixtures of ACV and glucosamine HCl, and the prepared ACV-SD formulations are presented in Table 3. Pure ACV exhibited aqueous solubility of  $\sim 14 \mu\text{g/mL}$ . This is not surprising, as ACV is a known BCS Class III ( $\uparrow$  solubility,  $\downarrow$  permeability) or class IV ( $\downarrow$  solubility,  $\downarrow$  permeability) drug (18). The results are in agreement with previously published aqueous solubility values for ACV (9, 41). The solubilities of ACV in the physical mixtures ranged between 82 and  $85 \mu\text{g/mL}$ . These values represented a nearly 6-fold higher solubility of ACV in the physical mixture compared to that of ACV alone. A close association of the water-soluble carrier resulting in an increased wetting efficiency of ACV particles in the aqueous medium is a likely cause for the observed higher aqueous solubility of ACV in the physical mixture. Among the physical mixtures, ACV-SD3 (drug-carrier ratio of 1:3) exhibited the highest observed solubility of ACV. Further increase in the ratio of carrier probably restricted ACV particles access to water, resulting in the observed modest decrease in ACV solubility (27). The prepared ACV-SD formulations exhibited significantly higher solubilities of ACV, compared to that of pure ACV or ACV in the physical mixtures. The solubilities of ACV in these formulations ranged between 165 and  $191 \mu\text{g/mL}$ . These results represented a nearly 12-fold increase in the solubility of ACV compared to that of ACV alone,

**Table 3** Aqueous solubility of pure acyclovir, acyclovir in physical mixture (PM), and acyclovir in the prepared solid-dispersions

FORMULATION	AQUEOUS SOLUBILITY ( $\mu\text{g/mL}$ )*
Pure acyclovir	$13.91 \pm 0.02$
PM-1	$82.25 \pm 0.03$
PM-2	$84.59 \pm 0.02$
PM-3	$85.11 \pm 0.08$
PM-4	$83.27 \pm 0.04$
PM-5	$84.40 \pm 0.03$
ACV-SD1	$165.15 \pm 0.02$
ACV-SD2	$171.28 \pm 0.08$
ACV-SD3	$191.33 \pm 0.06$
ACV-SD4	$183.49 \pm 0.06$
ACV-SD5	$180.36 \pm 0.07$

\*All results are expressed as mean  $\pm$  Std. Dev., n=3

and a 2-fold increase compared to that of ACV in the physical mixture. The solubilities of ACV within these formulations followed a trend similar to that observed with the physical mixtures. The observed enhanced aqueous solubility of ACV in these formulations may be attributed to carrier-assisted modifications of the physical-chemical properties of ACV such as changes in the particle size, morphology, and polymorphic state (26).

## Functional characterization of ACV-SD

### *In vitro* dissolution studies

The comparative dissolution profiles of pure ACV and the ACV-SD formulations prepared using different drug-carrier ratios, in phosphate buffer (0.05 M, pH 6.8) are represented in Figure 6. Pure ACV exhibited an initial rapid dissolution (~30% in 10 minutes), followed by a steady, zero-order release over a period of 2 hours. At the end of the dissolution period, the extent of cumulative ACV dissolution was recorded at

~62%. The relatively lower dissolution efficiency of pure ACV is attributable to its low aqueous solubility. The rate and extent of ACV dissolution from the prepared ACV-SD formulations followed the trend observed with the solubility studies, i.e., cumulative rate and extent of ACV dissolution increased in formulations with increasing drug-carrier ratio, up to the ratio of 1:3. For formulations with a drug-carrier ratio of 1:4 and 1:5 the cumulative dissolution of ACV was observed to be relatively slower and to a lesser extent. This is possibly due to the higher concentration of carrier inhibiting the access of ACV particles to the dissolution media (27). ACV-SD3 (drug-carrier ratio of 1:3) exhibited the highest observed rate and extent of ACV dissolution (~94%). Earlier studies suggested that solvent-evaporation-method-based solid dispersions produce high energy solid-state formulations by partial amorphization of drug particles, which increases the dissolution rate of drugs (17). Another possibility for explaining enhanced aqueous solubility may be the hydrophilic nature of glucosamine HCl increasing the

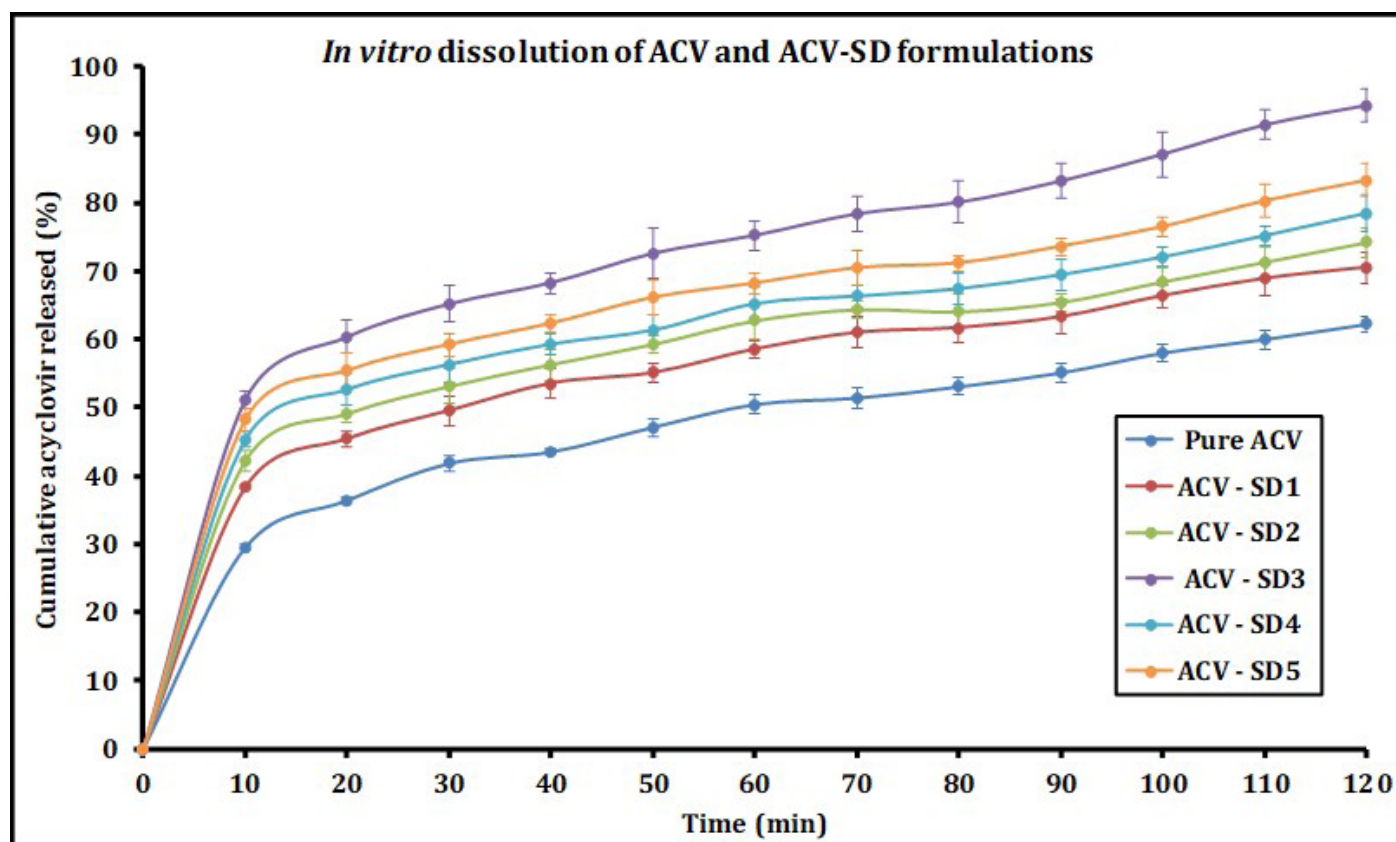


**Figure 6** The comparative *in vitro* dissolution profiles of ACV and ACV-SD3 formulations.



wettability of dispersed ACV particles in ACV-SD (26).

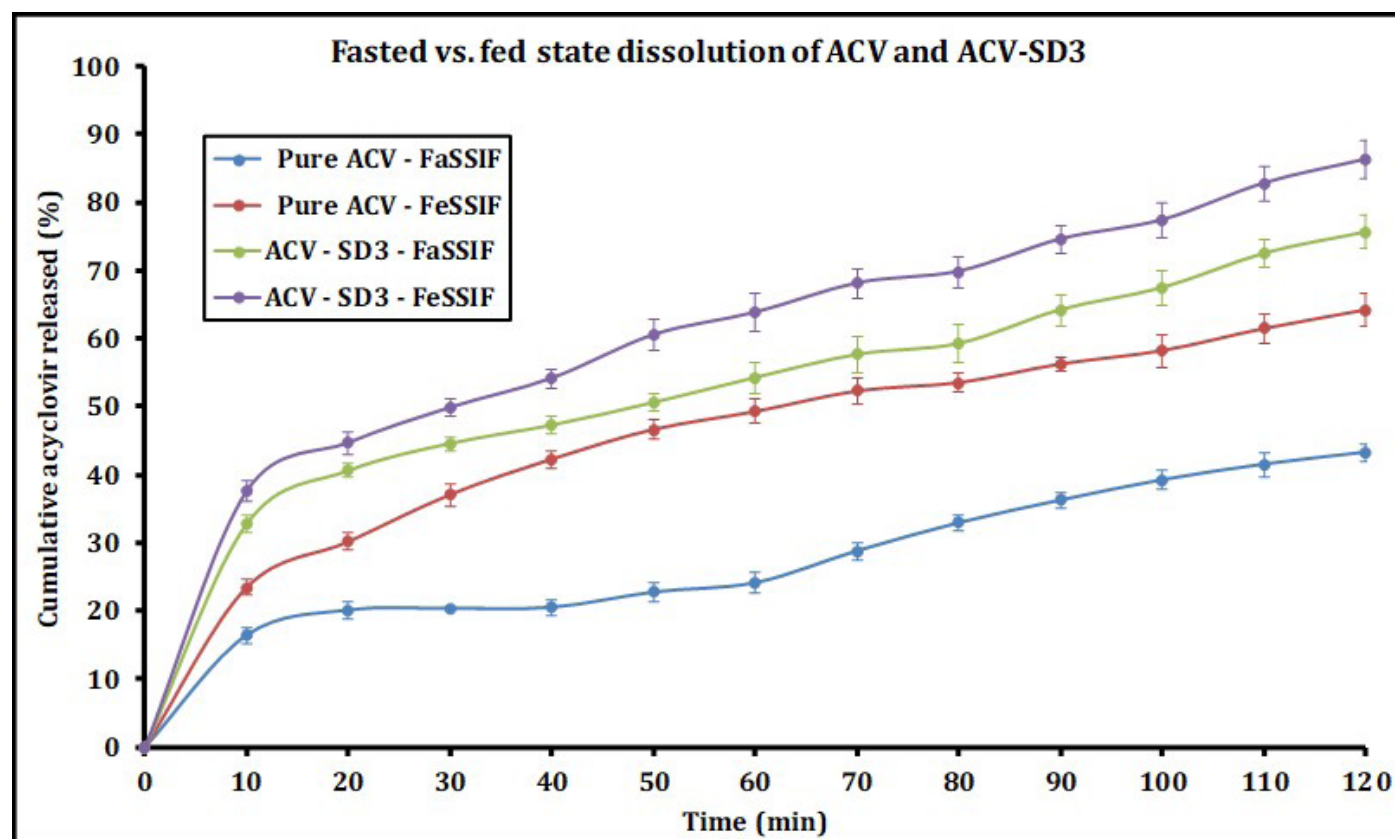
### **Influence of fasted versus fed state media**

Figure 7 shows a comparison of the dissolution profiles of pure ACV and that of ACV from ACV-SD3 formulation as tested in FaSSIF (fasted) and FeSSIF (fed) media. The efficiency of the dissolution of pure ACV was found to be lower in fasted conditions compared to that in fed conditions. At the end of the 2-hour dissolution period, only about 43% of pure ACV had dissolved. In fed conditions, there was a modest, albeit significant increase in the efficiency of ACV dissolution (~64% at the end of 2 hours). Positive food effects on the dissolution of drugs with low aqueous solubility have been reported earlier (32, 42). The rate and extent of ACV release from ACV-SD3 were found to be higher in both fasted and fed conditions compared to that of pure ACV. In fasted conditions ~76%, and in fed conditions ~84% ACV was released at the end of the 2-hour dissolution

period. These results correlated well with those obtained from the solubility analysis and the in vitro dissolution studies.

### **Permeability across a biological membrane**

The comparative permeabilities of pure ACV and ACV-SD formulations across a biological membrane, as evaluated by the everted rat intestine model are shown in Figure 8. After the 2-hour testing period, only about 42% of pure ACV had permeated across the membrane. ACV is reported at a BCS class III or IV drug (low permeability), and thus the results are consistent with those published previously (8, 18). The permeability profiles of ACV from all ACV-SD formulations were found to be relatively higher compared to that of pure ACV. The permeability of ACV from these formulations followed the trend observed with the results obtained from solubility and dissolution studies. In general, the rate and extent of ACV permeability increased with increasing



**Figure 7** The influence of fasted and fed-state conditions on the dissolution behavior of pure ACV and the ACV-SD formulations.



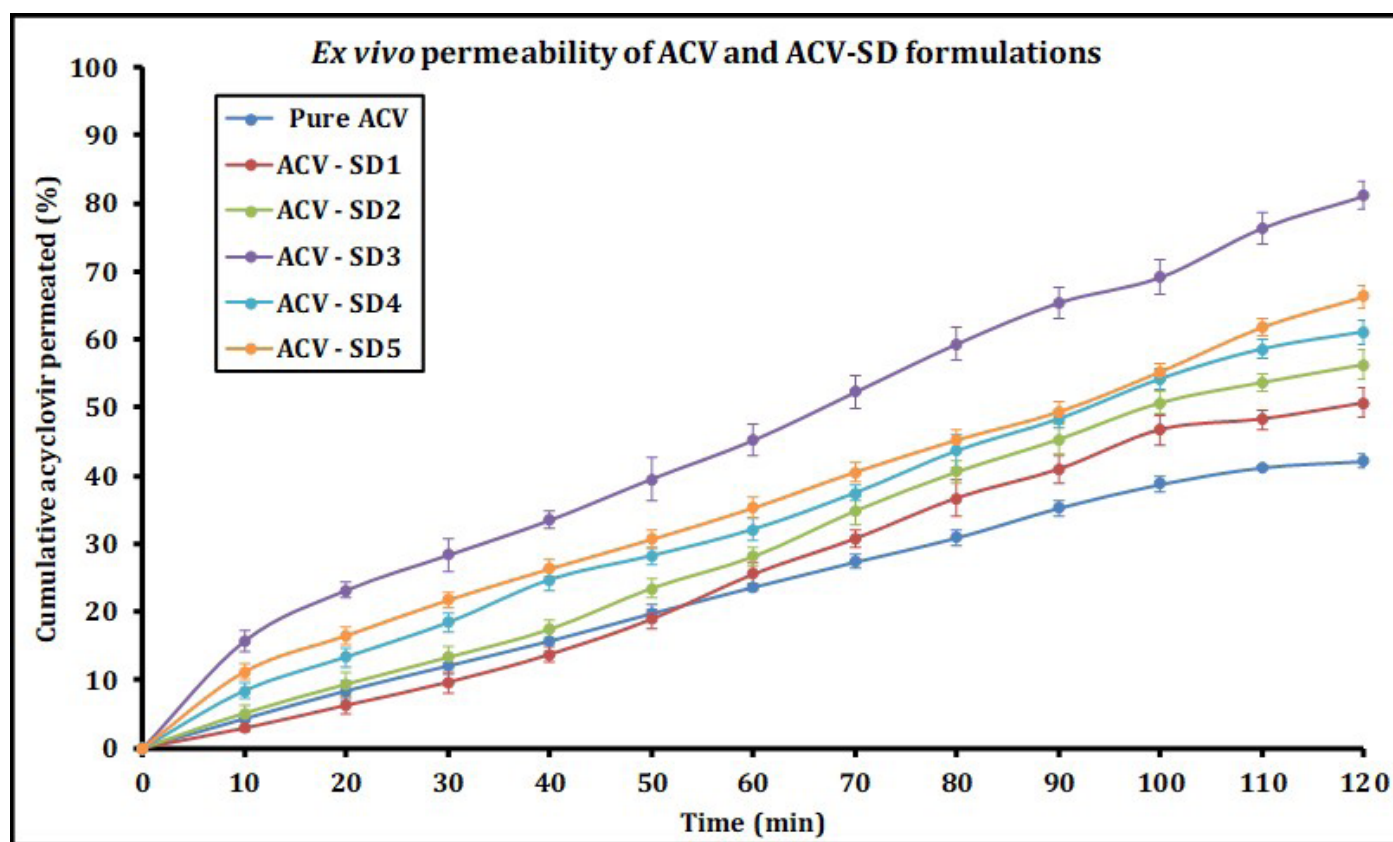


**Figure 8** The comparative ex vivo permeability profiles of the ACV and ACV-SD formulations.

drug-polymer ratio up to 1:3. ACV permeability was observed to be lower for formulations with a drug-carrier ratio of 1:4 and 1:5. ACV-SD3 (drug-carrier ratio of 1:3) exhibited the highest observed efficiency of ACV permeability.

### Preliminary stability assessment

The results obtained from the preliminary stability assessment of the selected ACV-SD3 formulation was stored at controlled temperature (25°C) and relative humidity ( $60 \pm 5\%$  RH) for 6 months are shown in Figure 9. Figure 9A shows a comparison of dissolution profiles of ACV-SD3 at day 0 and day 180 (6 months). It was observed that while the drug release from the 180-day sample followed a pattern similar to that of day 0 sample, there was a noticeable decrease in the efficiency of ACV dissolution at the end of the duration of the study. Figure 9B compares the permeability profiles of ACV-SD3 at day 0 and day 180. Similar to the dissolution results, there was a noticeable

decrease in the efficiency of ACV permeability for the samples stored for 180 days, whilst the permeability profile followed matching patterns. The reasons for this shift in the dissolution and permeability of ACV-SD are currently unclear. It is possible that the storage conditions, mainly the relative humidity have had an influence on the physical-chemical properties of ACV or the solid dispersion. Further characterization of the stored samples is currently underway.

### CONCLUSIONS

The present study aimed to study the feasibility of utilizing a relatively unexplored, hydrophilic excipient, glucosamine HCl as a solid-dispersion carrier with the goal of enhancing the biopharmaceutical properties of drugs with low aqueous solubility. Solid dispersion based formulations of acyclovir combined with glucosamine HCl were successfully prepared using a previously established solvent-evaporation method. The prepared formulations were characterized for

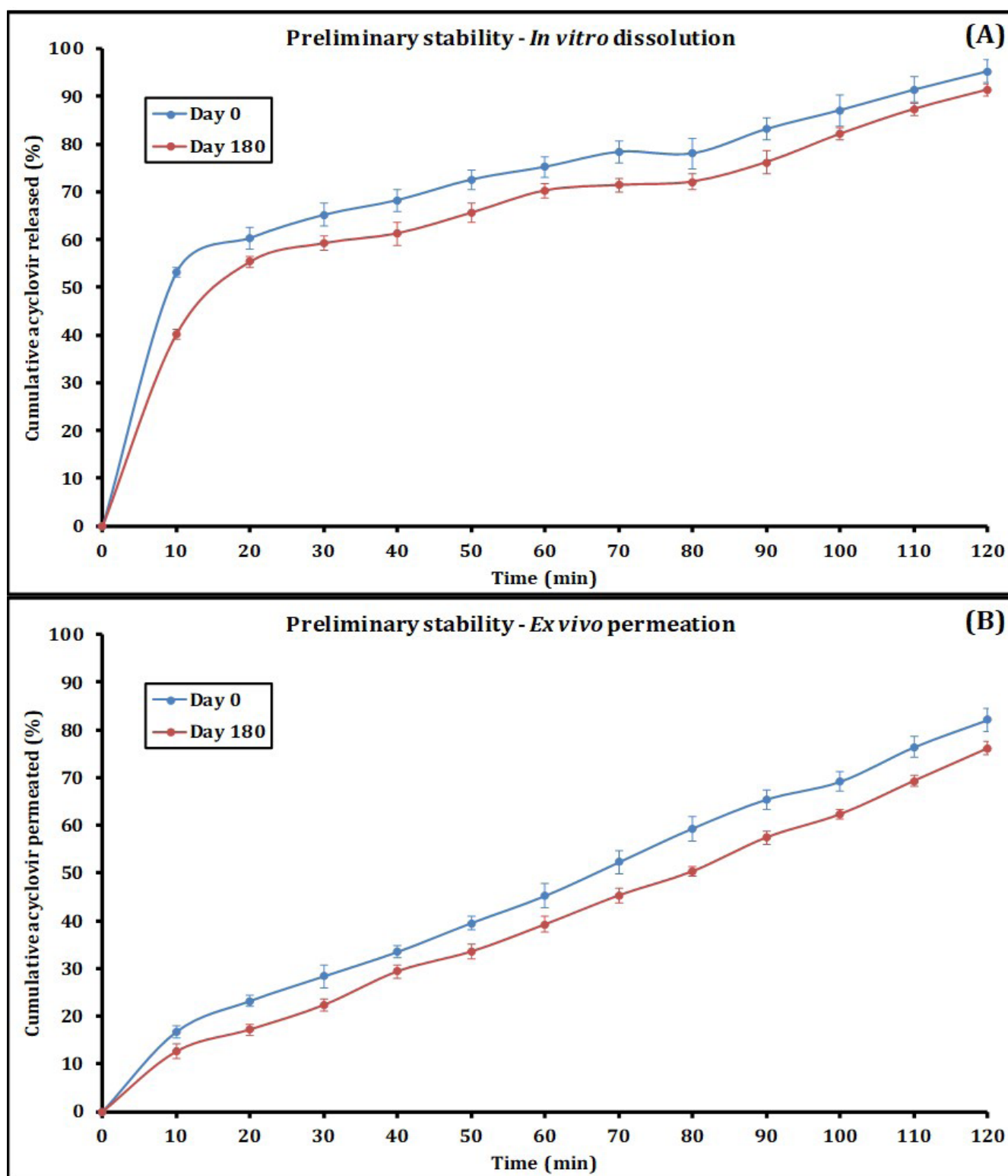


**Figure 9** The effect of controlled storage conditions (25°C/60% RH, 180 days) on (A) dissolution and (B) permeability of ACV-SD3.

their physical and functional properties using various analytical methods. The prepared ACV-glucosamine HCl solid dispersions demonstrated marked increases in aqueous solubility, dissolution, and permeability of acyclovir compared to the pure drug. The prepared solid dispersions were not found to be drastically unstable, the storage conditions appeared to have a modest influence on the physical-chemical properties of either the drug or the formulation. While the nature of this influence is unclear, further characterization of the stored samples is warranted. The study overall demonstrates the feasibility of utilizing glucosamine HCl as a potential solid-dispersion carrier to improve the biopharmaceutical properties of drugs with low solubility and/permeability characteristics.

## REFERENCES

- Shukla, D., et al., Lipid-based oral multiparticulate formulations - advantages, technological advances and industrial applications. *Expert Opin. Drug Deliv.*, 2011. 8(2): p. 207-24.
- Svenson, S., Dendrimers as versatile platform in drug delivery applications. *Eur. J. Pharm. Biopharm.*, 2009. 71 (3): p. 445-62.
- Kawabata, Y., et al., Formulation design for poorly water-soluble drugs based on biopharmaceutics classification system: Basic approaches and practical applications. *Int. J. Pharm.*, 2011. 420 (1): p. 1-10.
- Yu, L.X., et. al., Biopharmaceutics classification system: the scientific basis for biowaiver extensions. *Pharm. Res.*, 2002. 19 (7): p. 921-5.
- Rinaki, E., G. Valsami, and P. Macheras, Quantitative Biopharmaceutics Classification System: The Central Role of Dose/Solubility Ratio. *Pharm. Res.*, 2003. 20 (12): p. 1917-1925.
- Alsarra, I.A., A.Y. Hamed, and F.K. Alanazi, Acyclovir Liposomes for Intranasal Systemic Delivery: Development and Pharmacokinetics Evaluation. *Drug Delivery*, 2008. 15 (5): p. 313-321.
- Kharia, A.A. and A.K. Singhai, Development and optimisation of mucoadhesive nanoparticles of acyclovir using design of experiments approach. *J. Microencapsul.*, 2015. 32 (6): p. 521-32.
- Moniruzzaman, M., et. al., Ionic liquid-in-oil microemulsion as a potential carrier of sparingly soluble drug: Characterization and cytotoxicity evaluation. *Int. J. Pharm.*, 2010. 400 (1): p. 243-250.
- Nair, A.B., et. al., Enhanced oral bioavailability of acyclovir by inclusion complex using hydroxypropyl- $\beta$ -cyclodextrin. *Drug Delivery*, 2014. 21 (7): p. 540-547.
- Nart, V., et. al., Ball-milled solid dispersions of BCS Class IV drugs: Impact on the dissolution rate and intestinal permeability of acyclovir. *Materials Science and Engineering: C*, 2015. 53: p. 229-238.
- Rarokar, N.R., S.D. Saoji, and P.B. Khedekar, Investigation of effectiveness of some extensively used polymers on thermoreversible properties of Pluronic® tri-block copolymers. *Journal of Drug Delivery Science and Technology*, 2018. 44: p. 220-230.
- Rarokar, N.R., et. al., Nanostructured Cubosomes in a Thermoresponsive Depot System: An Alternative Approach for the Controlled Delivery of Docetaxel. *AAPS PharmSciTech*, 2016. 17 (2): p. 436-45.
- Shadab, et. al., Gastroretentive drug delivery system of acyclovir-loaded alginate mucoadhesive microspheres: formulation and evaluation. *Drug Deliv*, 2011. 18 (4): p. 255-64.
- Valizadeh, H., et. al., Physicochemical characterization of solid dispersions of indomethacin with PEG 6000, Myrj 52, lactose, sorbitol, dextrin, and Eudragit E100. *Drug Dev. Ind. Pharm.*, 2004. 30 (3): p. 303-17.
- Huang, Y. and W.-G. Dai, Fundamental aspects of solid dispersion technology for poorly soluble drugs. *Acta Pharmaceutica Sinica B*, 2014. 4 (1): p. 18-25.
- Serajuddin, A.T.M., Solid dispersion of poorly water soluble drugs: Early promises, subsequent problems, and recent breakthroughs. *J. Pharm. Sci.*, 1999. 88 (10): p. 1058-1066.
- Leuner, C. and J. Dressman, Improving drug solubility for oral delivery using solid dispersions. *Eur. J. Pharm. Biopharm.*, 2000. 50 (1): p. 47-60.
- Arnal, J., et. al., Biowaiver Monographs for Immediate Release Solid Oral Dosage Forms: Aciclovir. *J. Pharm. Sci.*, 2008. 97 (12): p. 5061-5073.
- Rottinghaus, S.T. and R.J. Whitley, Current non-AIDS antiviral chemotherapy. *Expert Rev. Anti Infect. Ther.*, 2007. 5 (2): p. 217-30.
- Bergström, C.A.S., et. al., Absorption Classification of Oral Drugs Based on Molecular Surface Properties. *J. Med. Chem.*, 2003. 46 (4): p. 558-570.
- Fletcher, C. and B. Bean, Evaluation of oral acyclovir therapy. *Drug Intell. Clin. Pharm.*, 1985. 19 (7-8): p. 518-24.
- Friedrichsen, G.M., et. al., Synthesis of analogs of l-valacyclovir and determination of their substrate activity for the oligopeptide transporter in Caco-2 cells. *Eur. J. Pharm. Sci.*, 2002. 16 (1): p. 1-13.
- Wagstaff, A.J., D. Faulds, and K.L. Goa, Aciclovir. A reappraisal of its antiviral activity, pharmacokinetic properties and therapeutic efficacy. *Drugs*, 1994. 47 (1): p. 153-205.
- da Camara, C.C. and G.V. Dowless, Glucosamine sulfate for osteoarthritis. *Ann. Pharmacother.*, 1998. 32 (5): p. 580-7.

- 25 Pujalte, J.M., E.P. Llavore, and F.R. Ylescupidéz, Double-blind clinical evaluation of oral glucosamine sulphate in the basic treatment of osteoarthritis. *Curr. Med. Res. Opin.*, 1980. 7(2): p. 110-14.
- 26 Al-Hamidi, H., et. al., Effect of glucosamine HCl on dissolution and solid state behaviours of piroxicam upon milling. *Colloids Surf. B Biointerfaces*, 2013. 103: p. 189-99.
- 27 Al-Hamidi, H., et. al., To enhance dissolution rate of poorly water-soluble drugs: glucosamine hydrochloride as a potential carrier in solid dispersion formulations. *Colloids Surf. B Biointerfaces*, 2010. 76 (1): p. 170-8.
- 28 Dhore, P.W., et. al., Enhancement of the aqueous solubility and permeability of a poorly water soluble drug ritonavir via lyophilized milk-based solid dispersions. *Pharm. Dev. Technol.*, 2017. 22 (1): p. 90-102.
- 29 Telange, D.R., et. al., Kaempferol-Phospholipid Complex: Formulation, and Evaluation of Improved Solubility, in vivo Bioavailability, and Antioxidant Potential of Kaempferol. *J. Excipients and Food Chem.*, 2016. 7 (4): p. 89-120.
- 30 Telange, D.R., et. al., Drug-phospholipid complex-loaded matrix film formulation for enhanced transdermal delivery of quercetin. *J. Excipients and Food Chem.*, 2018. 9 (2): p. 31-50.
- 31 Choudhary, A., et. al., Development and characterization of an atorvastatin solid dispersion formulation using skimmed milk for improved oral bioavailability. *Acta Pharmaceutica Sinica B*, 2012. 2(4): p. 421-428.
- 32 Klein, S., The use of biorelevant dissolution media to forecast the in vivo performance of a drug. *The AAPS journal*, 2010. 12 (3): p. 397-406.
- 33 Dixit, P., D.K. Jain, and J. Dumbwani, Standardization of an ex vivo method for determination of intestinal permeability of drugs using everted rat intestine apparatus. *J. Pharmacol. Toxicol. Methods*, 2012. 65 (1): p. 13-7.
- 34 Saoji, S.D., et. al., The role of phospholipid as a solubility- and permeability-enhancing excipient for the improved delivery of the bioactive phytoconstituents of *Bacopa monnieri*. *Eur. J. Pharm. Sci.*, 2017. 108: p. 23-35.
- 35 Lutker, K.M., et. al., Polymorphs and hydrates of acyclovir. *J. Pharm. Sci.*, 2011. 100 (3): p. 949-963.
- 36 Savic, R., et. al., Micellar nanocontainers distribute to defined cytoplasmic organelles. *Science*, 2003. 300 (5619): p. 615-8.
- 37 Karolewicz, B., et. al., Physicochemical characterization and dissolution studies of acyclovir solid dispersions with Pluronic F127 prepared by the kneading method. *Acta Pharm*, 2016. 66 (1): p. 119-28.
- 38 Gandhi, A., S. Jana, and K.K. Sen, In-vitro release of acyclovir loaded Eudragit RLPO((R)) nanoparticles for sustained drug delivery. *Int. J. Biol. Macromol.*, 2014. 67: p. 478-82.
- 39 Veerapandian, M., et. al., Copper-Glucosamine Microcubes: Synthesis, Characterization, and C-Reactive Protein Detection. *Langmuir*, 2011. 27 (14): p. 8934-8942.
- 40 Riekes, M.K., et. al., HPMC as a potential enhancer of nimodipine biopharmaceutical properties via ball-milled solid dispersions. *Carbohydr. Polym.*, 2014. 99: p. 474-82.
- 41 Liu, H., et. al., Preparation and evaluation of a novel gastric mucoadhesive sustained-release acyclovir microsphere. *Drug Dev. Ind. Pharm.*, 2010. 36 (9): p. 1098-105.
- 42 Raman, S. and J.E. Polli, Prediction of positive food effect: Bioavailability enhancement of BCS class II drugs. *Int. J. Pharm.*, 2016. 506 (1-2): p. 110-5.



## Quality by Design: A Roadmap for Quality Pharmaceutical Products

### Abstract

Quality by design (QbD) refers to a new approach to product development that could increase efficiencies, provide regulatory relief and flexibility, and offer important business benefits throughout the product life cycle. QbD is increasingly becoming an important and widely used technique in the pharmaceutical industry. QbD can be considered to be system-based approach to the design, development, and delivery of any product or service to a consumer. It is an approach to pharmaceutical development that begins with predefined objectives and emphasizes product and process understanding and process control. Process parameters and quality attributes are identified for each unit operation. Benefits, opportunities, and steps involved in QbD of pharmaceutical products are described. The aim of pharmaceutical development is to design a quality product and its manufacturing process to consistently deliver the intended performance of the product. Quality cannot be tested into products, but quality should be built in by design. It includes the quality target product profile, critical quality attributes, and key aspects of QbD. It also gives comparison between product quality by end product testing and product quality by QbD. The foundation of QbD is ICH guidelines. Hence, if we identify the cause and effect relationship between the various inputs and responses by carefully designed experiments, we can control the quality of the product by simply controlling the inputs such as raw material specifications or process parameters.

**Keywords:** Critical quality attributes, pharmaceutical manufacturing, process analytical technology, quality by design

### Introduction

Quality by design (QbD) means designing and developing formulations and manufacturing processes to ensure predefined product quality objectives. In pharmaceutical industry, QbD identifies characteristics that are critical to quality from the perspective of patients and health care team, translates them into the attributes that the drug product should possess, and establishes how the critical process parameters (CPPs) can be varied to consistently produce a drug product with the desired characteristics. The main concept of QbD is that all final product critical quality attributes (CQAs) are affected by raw materials and process parameters. Hence, if we identify the cause and effect relationship between the various inputs and responses, we can control the quality of the product by simply controlling the inputs such as raw material specifications or process parameters. As a result, the final product will always conform to the quality specifications.<sup>[1]</sup>

This is an open access journal, and articles are distributed under the terms of the Creative Commons Attribution-NonCommercial-ShareAlike 4.0 License, which allows others to remix, tweak, and build upon the work non-commercially, as long as appropriate credit is given and the new creations are licensed under the identical terms.

For reprints contact: [reprints@medknow.com](mailto:reprints@medknow.com)

In all cases, the product should be designed to meet patients' needs and the intended product performance. Strategies for product development vary from company to company and from product to product. The approach can also vary and should be outlined in the submission. An applicant might choose either an empirical approach or a more systematic approach to product development or a combination of both. A more systematic approach to development (also defined as QbD) can include, for example, incorporation of prior knowledge, results of studies using design of experiments, use of quality risk management (QRM), and use of knowledge management (ICH Q10) throughout the lifecycle of the product. Such a systematic approach can enhance achieving the desired quality of the product and help the regulators to better understand a company's strategy. Product and process understanding can be updated with the knowledge gained over the product lifecycle.<sup>[2]</sup>

### Quality by Design

This concept was first outlined by well-known quality expert Joseph M. Juran

**How to cite this article:** Chordiya MA, Gangurde HH, Sancheti VN. Quality by design: A Roadmap for quality pharmaceutical products. *J Rep Pharm Sci* 2019;8:289-94.

**Mayur Ashok Chordiya, Hemant Hiraman Gangurde, Vikram Nirmal Sancheti<sup>1</sup>**

*Department of Pharmaceutics, SNJB's Shriman Sureshdada Jain College of Pharmacy, Nashik, <sup>1</sup>Department of Pharmaceutics, Rajarshi Shahu College of Pharmacy, Buldana, Maharashtra, India*

### Address for correspondence:

*Dr. Mayur Ashok Chordiya, Department of Pharmaceutics, SNJB's Shriman Sureshdada Jain College of Pharmacy, Chandwad, Nashik, Maharashtra, India. E-mail: [chordiya.mayur@gmail.com](mailto:chordiya.mayur@gmail.com)*

### Access this article online

**Website:**  
[www.jrpsjournal.com](http://www.jrpsjournal.com)

**DOI:** 10.4103/jrptps.jrptps\_2\_18

### Quick Response Code:





on QbD (J.M.: “Juran on QbD”). With assistance of several biopharmaceutical companies, pilot programs were started to explore QbD application and understandings.<sup>[3]</sup>

As per ICH Q8 (R2) Pharmaceutical Development 2009, QbD is defined as “A systematic approach to development that begins with predefined objectives and emphasizes product and process understanding and process control, based on sound science and quality risk management.” It means designing and developing formulations and manufacturing processes to ensure predefined product quality objectives.<sup>[4]</sup>

### Benefits of Quality by Design

- QbD is good business<sup>[5]</sup>
- Eliminate batch failures
- Minimize deviations and costly investigations
- Avoid regulatory compliance problems
- Organizational learning is an investment in the future
- QbD is good science
- Better development decisions
- Empowerment of technical staff.

### Opportunities of Quality by Design

- Efficient, agile, flexible system
- Increase manufacturing efficiency, reduce costs, and project rejections and waste
- Build scientific knowledge base for all products
- Better interact with industry on science issues
- Ensure consistent information
- Incorporate risk management.

### Components of Quality by Design

#### Quality target product profile

The Food and Drug Administration (FDA) defines quality target product profile (QTPP) as the quality attributes related to safety and efficacy of the product. It may include route of administration, dosage form, delivery systems, dosage strength (s), container closure system, pharmacokinetic consideration, and drug product quality criteria (e.g. sterility, purity, stability, and drug release).<sup>[6]</sup>

It is important to acknowledge that QTPP should only include patient relevant product performance elements. For example, tablet density or hardness may be included as a specification for process monitoring but may not be included in QTPP. Furthermore, if particle size is critical to the dissolution of a solid oral product, then the QTPP should include dissolution but not particle size.

For a new drug application (NDA), the QTPP is under development, while for the abbreviated NDA (ANDA) product, the QTPP is well established based on the properties of the drug substance (DS), characterization of the reference listed drug (RLD) products, RLD label, and intended patient population. Therefore, a generic drug

product is expected to have the same QTPP as that of brand or reference product.<sup>[7]</sup>

### Critical quality attributes

Once QTPP has been identified, the next step is to identify the relevant CQAs. A CQA is defined as “a physical, chemical, biological, or microbiological property or characteristic that should be within an appropriate limit, range, or distribution to ensure the desired product quality.” This indicates that CQAs are subsets of QTPP that has a potential to be altered by the change in formulation or process variables. For example, QTPP may include additional quality attributes of the drug product such as strength and dosage form, which are not the part of CQA as it will not change during drug development process. However, QTPP attributes such as assay, content uniformity, dissolution, and permeation flux will also be a part of CQA as they may be altered by formulation or process variables.<sup>[8]</sup>

Identification of CQA can be performed based on prior knowledge and/or QRM. Prior knowledge may be attained by literature review, manufacturing experience, technology transfer, stability reports, raw material testing data, adverse event report, and recalls. QRM, on the other hand, applies various tools to identify and prioritize potential CQA.<sup>[9]</sup>

### Quality risk management

The FDA defines QRM as a systematic process for the assessment, control, communication, and review of risks to the quality of the drug product across the product life cycle. The goal of QRM is, therefore, to identify risks within a process or event, analyzing the significance of these risks, and takes appropriate measures to mitigate such risks if deemed unacceptable.<sup>[10]</sup>

QRM is integral part of QbD as it helps in identifying the extent of the impact of critical material attributes (CMA) and CPP on CQAs, which can eventually assist in prioritizing the CQAs. They are particularly important in complex processes, especially which are involved in cases of biologics or biosimilar. The FDA suggests various tools that can be applied for QRM, among which the relevant ones are discussed below:

#### Failure mode effects analysis

Failure mode effects analysis is one of the most commonly used risk assessment tools in the pharmaceutical industry. It is a systematic and proactive method to identify and mitigate the possible failure in the process. Failure modes represent any errors or defects in a process, material, design, or equipment. Once failure modes are established, FMEA tool evaluates the effect of these failures and prioritizes them accordingly. Risk control activities can then be performed to avoid such failure modes. Since FMEAs require a good understanding of cause and effects, a thorough process understanding is essential.<sup>[11,12]</sup>

### *Fault tree analysis*

The fault tree analysis (FTA) was first introduced by Bell Laboratories and is one of the most widely used methods in system reliability, maintainability, and safety analysis. FTA is a deductive analysis approach for resolving an undesired event into its causes in a top-down fashion. Typically, assumed failures are listed at the top as a main event and all of the associated elements in that system that could cause the event are listed as subsequent branches till the root condition or cause is identified. The results are represented pictorially in the form of a tree of fault modes and their relationship is described with logical operators such as “AND” and “OR.”<sup>[13]</sup>

### *Hazard Analysis and Critical Control Points*

The Hazard Analysis and Critical Control Points (HACCP) provides detailed documentation to show process or product understanding through identifying parameters to control and monitor.<sup>[14]</sup> The definition of hazard includes both safety and quality concern in a process or product. Examples of hazards within the pharmaceutical setting include environmental aspects of the facility (environmental conditions and hygiene aspects), material flow, manufacturing steps, personnel hygiene and gowning, and technical aspects relating to process design. HACCP consists of the following seven steps:

- (i) Conduct a hazard analysis and identify preventive measures for each step of the process
- (ii) Determine the critical control points
- (iii) Establish critical limits
- (iv) Establish a system to monitor the critical control points
- (v) Establish the corrective action to be taken when monitoring indicates that the critical control points are not in a state of control
- (vi) Establish system to verify that the HACCP system is working effectively
- (vii) Establish a record-keeping system.

### *Design space*

A design space is a multidimensional combination of input variables (e.g. material attributes), their interactions, and process parameters that have been demonstrated to provide assurance of quality. A design space may be constructed for a single unit operation, multiple unit operations, or for the entire process. Although according to the FDA guideline, defining design space is optional since the product and process understanding can be established without a formal design space, nevertheless, such approach can assist to better understanding and attain overall control of a system.<sup>[15]</sup>

In this regard, one can apply one-factor-at-time approach, which varies only one factor or variable at a time while keeping others constant. However, design of experiments (DoE) approach that varies

several input variables simultaneously is more efficient when studying two or more factors. Factorial designs (full or fractional) and the response surface methodology are characteristic tools for this kind of application. The key advantages of using DoE approach are summarized as follows:

- Exhaustive information from a minimum number of experiments
- Study effects individually by simultaneously varying all operating parameters
- Can account for variability in experiments, process, materials, or operators
- Able to provide understanding about the interaction between various variables
- Determine acceptable ranges of CPPs contributing to identification of a design space.

Basic steps involved in DoE approach are as follows:

#### *Defining input and output variables and range*

Based on prior knowledge and risk assessment, the input variables and their range can be defined. Screening design like full or fractional factorial design can also be utilized to identify the range of various variables. The response variable should be a CQA or closely related to them.<sup>[16,17]</sup>

#### *Select appropriate experimental design and perform the run*

The choice of experimental design may depend on the purpose of the study (e.g. a screening, optimization, or robustness study) and the factors and interactions involved in the studied and available resources (e.g. literature knowledge, time, labor, cost, and materials).<sup>[18,19]</sup>

#### *Model diagnostic*

After obtaining the initial model, foremost step is to check whether the model is appropriate or not. In general, the significance of a parameter is verified using the analysis of variance (ANOVA) method. ANOVA is a statistical method based on the *F*-test to estimate the significance of model terms. It involves subdividing the total variation of a data set into variation due to main effects, interaction, and residual error. Model terms can be added or eliminated from the analysis, depending on their significance. The new model, with more or fewer model terms, is again forced through this cycle until all terms included in the model satisfy *F*-test statistics.<sup>[20,21]</sup>

Once the overall model satisfies an ANOVA check, the next step is to determine what cannot be modeled (i.e. the errors resulting from the model). This is done using a residual analysis technique.<sup>[22]</sup>

#### *Illustration of design space*

The design space can be tabulated or graphically displayed using various methods. Graphically, the design space can

be illustrated by the following:

- Contour plots: A contour plot is a graphic representation of the relationships among three numeric variables in two dimensions. Two variables are for X-and Y-axes, and a third variable Z is for contour levels. You can interactively identify, label, color, and move contour levels, and change the resolutions of rectangular grids to get better contouring quality and performance
- Three-dimensional plots: These plots are used to illustrate and study the effect of two input variables on an output variable simultaneously. These plots are ideal for showing the process shape; however, contour plots are more useful for determining or displaying acceptable operating ranges for process parameters
- Overlay plots: When there is more than one quality characteristic in the design space, the use of overlay plots is helpful. The overlay window shows the design space, which indicates the various combinations of the factors that will provide results within the acceptable range.<sup>[23]</sup>

From the FDA perspective, regulatory submission in regard to design space should include the following aspects:

- Description of design space, including critical and other relevant parameters. The design space can be presented as ranges of material inputs and process parameters and graphical representations (contour, interaction or overlay plots) or through more complex mathematical relationships
- The interaction of various input variables (e.g. material attributes and/or process parameters) and their relationship with the CQAs. Interaction plots can be used to illustrate these relationships
- Data supporting justification of design space, which can include but not limited to historic knowledge base, conclusions from QRM, and experimental studies
- The relationship between the proposed design space and other unit operations or process steps
- Results and conclusions of the studies, if any, of a design space across different scales
- Justification that the control strategy ensures that the manufacturing process is maintained within the boundaries defined by the design space.

### Control strategies

ICH Q10 defines a control strategy as “a planned set of controls derived from current product and process understanding that assures process performance and product quality.<sup>[24]</sup> The controls can include parameters and attributes related to drug substance and drug product materials and components, facility and equipment operating conditions, in process controls, finished product specifications and the associated methods and frequency of monitoring and control.” A control strategy ensures that the process is maintained within the boundaries described by design space.

Specifically, the control strategy may include:

1. Control of input material attributes (e.g. DS, excipients, and primary packaging materials) based on an understanding of their impact on processability or product quality
2. Product specifications
3. Procedural controls
4. Facility controls, such as utilities, environmental systems, and operating conditions
5. Controls for unit operations that have an impact on downstream processing or end product quality (e.g. the impact of drying on degradation, particle size distribution of the granulate on dissolution)
6. A monitoring program (e.g. full product testing at regular intervals) for verifying multivariate prediction models.

It is important to appreciate that when developing a control strategy, a manufacturer can consider implementing single or multiple points of control for a specific CQA, depending on the risk associated with the CQA and the ability of individual controls to detect a potential problem. For example, with sterilized DSs or biotechnological/biological products, there is an inherent limitation in the ability to detect low levels of bacterial or viral contamination in the DS. In these cases, end product testing is considered to provide inadequate assurance of quality, so additional points of control (e.g. attribute and in-process controls) are incorporated into the control strategy.<sup>[25]</sup>

### Quality by Design and Abbreviated New Drug Application

Historically, FDA ensured high quality of generic drug products by requiring two fundamental evidence during ANDA filling pharmaceutical equivalence and bioequivalence. Drug products are considered pharmaceutical equivalents if they contain the same active ingredient (s) are of the same dosage form, route of administration, and strength or concentration. Bioequivalence, on the other hand, refers that the rate and extent of absorption of the test drug have no significant difference with that of the reference drug, when administered at the same molar dose under similar experimental conditions in either a single dose or multiple doses.<sup>[26]</sup>

While this approach has been successful, it should be acknowledged that majority of generic drug products approved under this paradigm were solution and immediate release oral products, which are inherently simple in design.<sup>[27]</sup>

However, three key observations were found in the recent QbD-based ANDA filling:

1. Exhaustive information being presented with no justification or interpretation of data. Often, there were no conclusions from the data presented
2. Improper use of basic QbD terminology, such as CQAs, CPPs, and in particular, design space

3. Prior knowledge is often presented without necessary context.

Such issues may indicate an ineffective communication and collaboration between FDA and generic drug companies in regard to QbD implementation. It is expected that as the time will progress, more effective knowledge database will be developed and communicated from both sides that can help in resolving these critical issues.<sup>[28]</sup>

### Advantage of Implementing Quality by Design

1. The ability to design products and processes and bring fewer setbacks at critical stages such as scale-up, validation, and transfer
2. Since the operation is working in a well-defined design space, it allows greater flexibility of adjusting variables within such space
3. Greater regulatory flexibility based on a science-based approach to risk management
4. Ability to continue to optimize and improve the manufacturing operation without facing additional regulatory filings or scrutiny
5. Faster time to market and reduced rework, resulting in reduced costs and increased revenues.<sup>[29,30]</sup>

### Challenges

1. Lack of understanding regarding the QbD is the cause and also the major limitation for QbD implementation. Pharmaceutical companies are traditionally tuned to care more about the end product, with little emphasis on the science-based understanding of the process involved
2. Collaboration and consensus between field inspectors and the FDA review and compliance sectors on how to handle QbD remains an unmet challenge
3. The majority of pharmaceutical companies feel that there is a need for more tangible guidance on how to actually implement QbD. Companies want clarification from the FDA on QbD terminologies, acceptable methods, criteria to select and deselect CQAs, standards by which to judge adequacy of controls, and criteria for analytical method substitution
4. There is a need for greater cooperation across multiple disciplines within the company, including process development, manufacturing, and quality control for effective implementation of QbD
5. Pharmaceutical companies also feel that QbD would decrease time to file approval application or could provide unnecessary information to the regulatory authority that might create an obstacle in the approval process.<sup>[31]</sup>

### Conclusion

The goal of a well-characterized method development effort is to develop a reliable method that can be demonstrated with a high degree of assurance to consistently produce

data meeting predefined criteria when operated within defined boundaries. QbD can be applied to the development and evaluation of analytical methods.

QbD is a common understanding on the concepts of ICH Q8, Q9, and Q10 and will be essential in the process of formulation. It also explains application of QbD principles and tools to drug product and process development. It can be concluded that QbD principles and tools play an important role in facilitating a higher level of process understanding and create opportunities for investigation and developed control strategies in formulation and process development.

The regulatory authorities also need to harmonize the regulatory requirement. It is accepted that the challenges and concerns associated with the implementation of QbD can only be resolved if there is efficient communication between the industry and the regulatory bodies.

### Financial support and sponsorship

Nil.

### Conflicts of interest

There are no conflicts of interest.

### References

1. Mollah H, Baseman H, Long M. Risk Management Applications in Pharmaceutical and Biopharmaceutical Manufacturing. New Jersey: Wiley; 2013.
2. Chordiya M, Senthilkumaran K. Cyclodextrin in drug delivery: A review. *Res Rev J Pharm Pharma Sci* 2012;1:19-29.
3. US Food and Drug Administration. Guidance for Industry: Q9 Quality Risk Management. US Department of Health and Human Service. Rockville, MD: US Food and Drug Administration; 2006.
4. Rathore AS, Winkle H. Quality by design for biopharmaceuticals. *Nat Biotechnol* 2009;27:26-34.
5. Chordiya M, Gangurde H, Borkar V. Technologies, optimization and analytical parameters in gastroretentive drug delivery systems. *Curr Sci* 2017;112:946-53.
6. Chang RK, Raw A, Lionberger R, Yu L. Generic development of topical dermatologic products, part II: Quality by design for topical semisolid products. *AAPS J* 2013;15:674-83.
7. Yu LX. Pharmaceutical quality by design: Product and process development, understanding, and control. *Pharm Res* 2008;25:781-91.
8. Looby M, Ibarra N, Pierce JJ, Buckley K, O'Donovan E, Heenan M, *et al.* Application of quality by design principles to the development and technology transfer of a major process improvement for the manufacture of a recombinant protein. *Biotechnol Prog* 2011;27:1718-29.
9. Yu LX, Lionberger R, Olson MC, Johnston G, Buehler G, Winkle H. Quality by design for generic drugs. *Pharma Technol* 2009;33:122-7.
10. Lionberger RA, Lee SL, Lee L, Raw A, Yu LX. Quality by design: Concepts for ANDAs. *AAPS J* 2008;10:268-76.
11. Adam S, Suzzi D, Radeke C, Khinast JG. An integrated quality by design (QbD) approach towards design space definition of a blending unit operation by discrete element method (DEM) simulation. *Eur J Pharm Sci* 2011;42:106-15.



Chordiya, *et al.*: Quality by design (QbD)

12. US Food and Drug Administration. Guidance for industry: Q8(R2) Pharmaceutical Development. US Department of Health and Human Service. Rockville, MD: US Food and Drug Administration; 2009.
13. US Food and Drug Administration. Quality by Design for ANDAs: An Example for Immediate-Release Dosage Forms. US Department of Health and Human Service. Rockville, MD: US Food and Drug Administration; 2012.
14. McConnell J, McGarvey B, Nunnally B. Quality risk management and variability reduction. *J Validation Tech* 2011;11:12-6.
15. Fahmy R, Kona R, Dandu R, Xie W, Claycamp G, Hoag SW. Quality by design I: Application of failure mode effect analysis (FMEA) and Plackett-Burman design of experiments in the identification of "main factors" in the formulation and process design space for roller-compacted ciprofloxacin hydrochloride immediate-release tablets. *AAPS PharmSciTech* 2012;13:1243-54.
16. Trivedi B. Quality by design (QbD) in pharmaceuticals. *Int J Pharm Pharm Sci* 2012;4:17-29.
17. US Food and Drug Administration. Guidance for Industry: Q11 Development and Manufacture of Drug Substances. US Department of Health and Human Service. Rockville, MD: US Food and Drug Administration; 2012.
18. Raw AS, Lionberger R, Yu LX. Pharmaceutical equivalence by design for generic drugs: Modified-release products. *Pharm Res* 2011;28:1445-53.
19. Wu H, White M, Khan MA. Quality-by-design (QbD): An integrated process analytical technology (PAT) approach for a dynamic pharmaceutical co-precipitation process characterization and process design space development. *Int J Pharm* 2011;405:63-78.
20. White E. Risk management for aseptic processing. *J Validation Technol* 2009;15:25-33.
21. Gad SC, editor. *Handbook of Pharmaceutical Biotechnology*. New Jersey: Wiley; 2007.
22. Frank T, Brooks S, Murray K, Reich S, Sanchez E, Hasselbalch B, *et al.* Defining process design space: A risk-management case study (Part I). *Pharma Technol* 2011;35:77-9.
23. Keizer JA, Vos JP, Halman JJ. Risks in new product development: Devising a reference tool. *R D Manage* 2005;35:297-309.
24. Altan S, Bergum J, Pfahler L, Senderak E, Sethuraman S, Vukovinsky KE. Statistical considerations in design space development part I of III. *Pharma Technol* 2010;34:66-70.
25. Harms J, Wang X, Kim T, Yang X, Rathore AS. Defining process design space for biotech products: Case study of *Pichia pastoris* fermentation. *Biotechnol Prog* 2008;24:655-62.
26. Huang J, Kaul G, Cai C, Chatlapalli R, Hernandez-Abad P, Ghosh K, *et al.* Quality by design case study: An integrated multivariate approach to drug product and process development. *Int J Pharm* 2009;382:23-32.
27. Sancheti VN, Chordiya MA, Senthilkumaran K. Development and *in vitro* evaluation of bilayer elementary osmotic tablet of verapamil hydrochloride. *Am J Pharm Health Res* 2014;3:199-210.
28. Altan S, Bergum J, Pfahler L, Senderak E, Sethuraman S, Vukovinsky KE. Statistical considerations in design space development part II of III. *Pharma Technol* 2010;34:52-60.
29. Shivhare M, McCreath G. Practical considerations for doe implementation in quality by design. *Bio Process Int* 2010;8:22-30.
30. Korakianiti E, Rekkas D. Statistical thinking and knowledge management for quality-driven design and manufacturing in pharmaceuticals. *Pharm Res* 2011;28:1465-79.
31. US Food and Drug Administration. Guidance for industry Q8, Q9, and Q10 Questions and Answers. US Department of Health and Human Service. Rockville, MD: US Food and Drug Administration; 2012.